{HNS-MS}

Improving Member States preparedness
to face an HNS pollution of the Marine System

Modelling drift, behaviour and fate of HNS maritime pollution

HNS-MS final report, part II

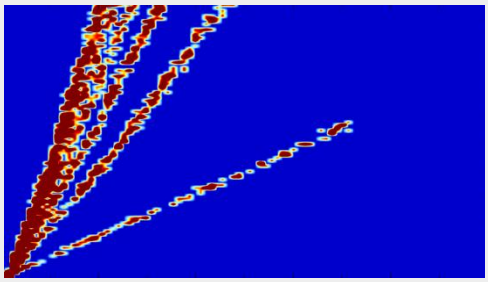

HNS floater from sunken vessel

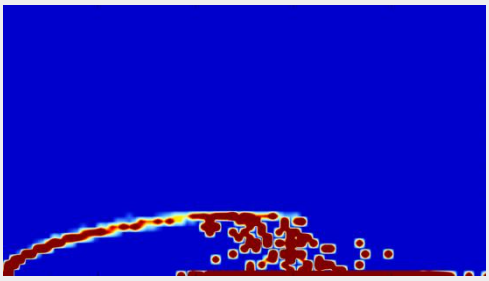

HNS sinker from sunken vessel

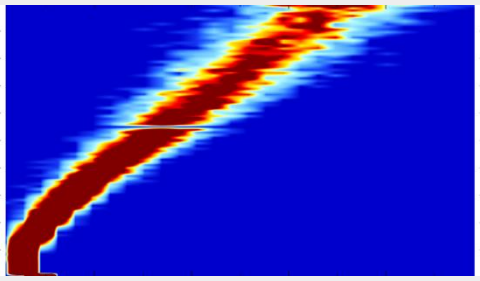

Gas release from pipeline break

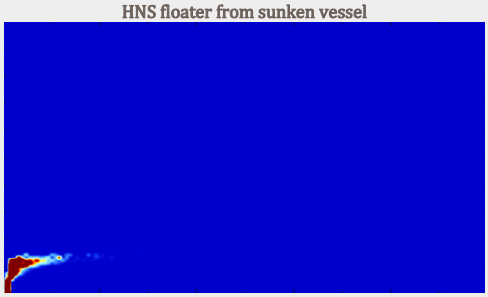

HNS dissolver from sunken vessel

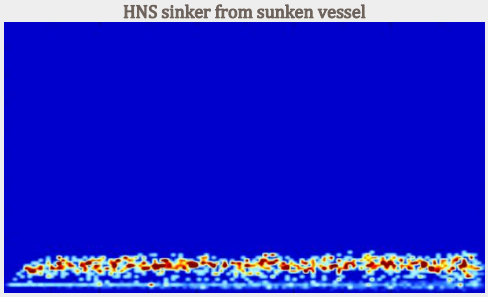

Dissolved HNS/water aqueous solution

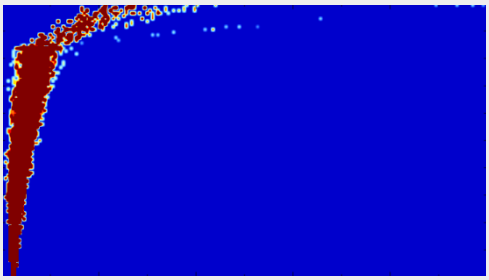

HNS floater from a well blowout

museum
Operational Directorate Natural Environment
OD Nature | OD Natuur | DO Nature

Cedre

ARMINES

ALYOTECH

federal public service
HEALTH, FOOD CHAIN SAFETY AND ENVIRONMENT

HNS-MS is a project co-funded by DG-ECHO under agreement ECHO/SUB/2014/693705.
It runs from 1 January 2015 to 31 March 2017.

HNS-MS contributors

Sébastien Legrand[1], Florence Poncet[2], Laurent Aprin[3], Valérie Parthenay[4], Eric Donnay[5], Gabriel Carvalho[2], Sophie Chataing-Pariaud[2], Gilles Dusserre[3], Vincent Gouriou[2], Stéphane Le Floch[2], Pascale Le Guerroue[2], Yann-Hervé Hellouvry[4], Frédéric Heymes[3], Fabrice Ovidio[1], Samuel Orsi[1], José Ozer[1], Koen Parmentier[1], Rémi Poisvert[4], Emmanuelle Poupon[2], Romain Ramel[4], Ronny Schallier[1], Pierre Slangen[3], Amélie Thomas[2], Vassilis Tsigourakos[2], Maarten Van Cappellen[1], Nabil Youdjou[1].

(1) Royal Belgian Institute of Natural Sciences
(2) CEDRE
(3) ARMINES, Ecole des Mines d'Alès
(4) Alyotech France
(5) Belgian FPS Health, food chain safety and environment

Citation

Legrand S., F. Poncet, L. Aprin, V. Parthenay, E. Donnay, G. Carvalho, S. Chataing-Pariaud, G. Dusserre, V. Gouriou , S. Le Floch, P. Le Guerroue, Y.-H. Hellouvry, F. Heymes, F. Ovidio, S. Orsi, J.Ozer, K. Parmentier, R. Poisvert, E. Poupon, R. Ramel, R. Schallier, P. Slangen, A. Thomas, V. Tsigourakos, M. Van Cappellen and N. Youdjou (2017) "Modelling drift, behaviour and fate of HNS maritime pollution ", HNS-MS final report, part II, 104 pp.

About HNS-MS

The European project HNS-MS aimed at developing a decision-support system that national maritime authorities and coastguard stations can activate to forecast the drift, fate and behaviour of acute marine pollution by Harmful Noxious Substances (HNS) accidentally or deliberately released in the marine environment. Focussing on the Greater North Sea and Bay of Biscay, this 27 months project (01/01/2015-31/03/2017) had four specific objectives:

i. To develop a freely accessible data base documenting the most important HNS transported from or to the ports of Antwerp, Rotterdam, Hamburg, Nantes and Bordeaux;
ii. To conduct lab experiments in order to improve the understanding of the physico-chemical behaviour of HNS spilt at sea;
iii. To develop a 3D mathematical modelling system that can forecast the drift, fate and (SEBC) behaviours of HNS spilt at sea. Advanced processes such as chemical reactivity, explosions, fire or interaction with sediment were not considered in this first project;
iv. To produce environmental and socioeconomic vulnerability maps dedicated to HNS that will help end-users assessing the likely impacts of HNS pollution on the marine environment, human health, marine life, coastal or offshore amenities and other legitimate uses of the sea.

All these contributions have been integrated into a web application that will help coastguard stations to evaluate the risks for maritime safety, civil protection and marine environment in case of an acute pollution at sea. HNS-MS has been co-funded by the Directorate-General of European Commission for European Civil Protection and Humanitarian Aid Operations (ECHO).

About this report

This report presents the achievements of the lab experiments carried out in the framework of tasks F, G and H of the project "HNS-MS – Improving Member States preparedness to face an HNS pollution of the Marine System".

This report is part of a series of 5 technical sub-reports presenting in detail the outcome achieved by the HNS-MS consortium in the framework of this project:

- HNS-MS Layman's report
- Sub-report I : Understanding HNS behaviour in the marine environment
- Sub-report II : Modelling drift, behaviour and fate of HNS maritime pollution
- Sub-report III : Mapping HNS environmental and socioeconomic vulnerability to HNS maritime pollution
- Sub-report IV : HNS-MS Decision-Support System User's Guide

A copy of these reports can be obtained by downloading from the HNS-MS website https://www.hns-ms.eu/publications/.

Contents

Introduction

PAGE INTENTIONALLY LEFT BLANK

1 Introduction

1.1 General context

"*Maritime services have benefited in recent years by considerable expansion fostered by globalization.*"[1] "*Around 90% of world trade is carried by the international shipping industry. Without shipping the import and export of goods on the scale necessary for the modern world would not be possible. Seaborne trade continues to expand, bringing benefits for consumers* across the world through competitive freight costs. Thanks to the growing efficiency of shipping *as a mode of transport and increased economic liberalisation, the prospects for the industry's further growth continue to be strong.*" [2]

If maritime shipping is undoubtedly a key factor of the worldwide economic growth, the constantly growing fleet of tankers, bulk carriers and ever-increasing size container ships exacerbates the risk of maritime accidents, loss of cargoes and acute maritime pollution. In particular, more than 2,000 **harmful or noxious chemical substances** (**HNS**) are regularly shipped in bulk or package forms and can potentially give rise to significant environmental and/or public health impacts in case of spillage in the marine environment.

In recent years, huge efforts have been made by IMO, EMSA as well as other maritime authorities towards greater consideration of these risks. For instance, given the importance and complexity of the matter, the Bonn Agreement, HELCOM, Lisbon Convention, Barcelona Convention/REMPEC, Copenhagen Convention, DG ECHO and EMSA have jointly identified the urgent need of improving preparedness and response to HNS spills (10th Inter-Secretariat Meeting, Helsinki, 27.02.2014).

Until now, preparedness actions at various levels have primarily aimed at classifying the general environmental or public health hazard of an HNS (e.g. development of IBC and IMDG codes; GESAMP profiles), at developing operational datasheets collating detailed, substance-specific information for responders and covering information needs at the first stage of an incident. (MAR-CIS; MIDSIS-TROCS; CAMEO) or at performing a risk analysis of HNS transported in European marine regions (e.g. EU projects HASREP and BE-AWARE). However, contrary to oil pollution preparedness and response tools, only few decision-support systems currently used by Member States authorities (Coastguard agencies or other) integrate 3D models that are able to simulate the drift, fate and behaviour of HNS spills in the marine environment. When they do, they usually rely on black box commercial software or consider simplified or steady-state environmental conditions.

[1] World Trade Organization - https://www.wto.org/english/tratop_e/serv_e/transport_e/transport_maritime_e.htm
[2] International Chamber of Shipping - http://www.ics-shipping.org/shipping-facts/shipping-and-world-trade

HNS-MS aims at developing a 'one-stop shop' integrated decision-support system that is able to predict the drift, fate and behaviour of HNS spills under realistic environmental conditions and at providing key product information - drawing upon and in complement to existing studies and databases - to improve the understanding and evaluation of a HNS spill situation in the field and the environmental and safety-related issues at stake.

The key challenge in this project is to understand the physico-chemical processes that drive the numerous behaviours and fate of HNS spilt in the marine environment.

1.2 What are HNS precisely?

HNS-MS defines **hazardous and noxious substances** or **HNS** following the OPRC-HNS Protocol 2000:

> *"HNS are any substances other than oil which, if introduced into the marine environment, are likely to create hazards to human health, to harm living resources and marine life, to damage amenities or to interfere with other legitimate uses of the sea".*

This generic definition covers a wide range of chemicals with diverse intrinsic qualities (such as toxicity, flammability, corrosiveness, and reactivity with other substances or auto-reactivity). It includes:

- oil derivatives;
- liquid substances which are noxious or dangerous;
- liquefied gases;
- liquids with flashpoints not exceeding 60°C;
- packaged dangerous, harmful and hazardous materials; and
- solid bulk material with associated chemical hazards.

In the framework of HNS-MS, vegetal oils are also considered as HNS.

1.3 How does HNS behave when spilt in the marine environment?

The behaviour of a substance spilt at sea is the way in which it is altered during the first few hours after coming into contact with water. Predicting this behaviour is one of the most important stages in the development of a response strategy.

Since the early 1990's, the best HNS behaviours predictions were given by the Standard European Behaviour Classification (SEBC) [Bonn Agreement, 1991]. This classification determines the theoretical behaviour of a substance according to its density, vapour pressure and solubility. Five main behaviour classes are considered: **gas**, **evaporator**, **floater**, **dissolver** and

sinker. However, most of the time, a substance does not have one single behaviour but rather several behaviours due to its nature and the environmental conditions (wind, waves, current). This is the reason why the SEBC considers a total of 12 mixed behaviours classes (**Error! Reference source not found.**). For example, ethyl acrylate is classified as FED as it floats, evaporates and dissolves.

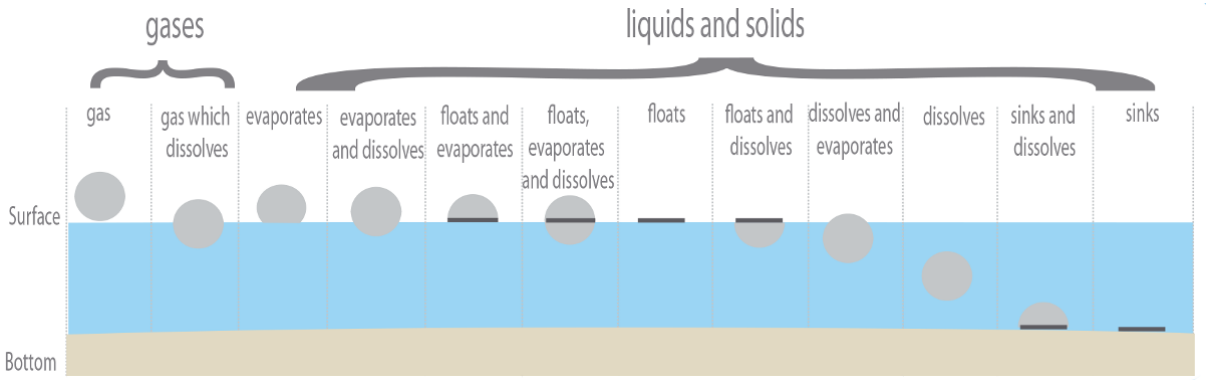

Figure 1: According the Standard European Behaviour Classification (SEBC), a substance spilt at sea will behave following one of these 12 theoretical behaviour classes.

The SEBC code has its limits. It is based on experiments conducted in the laboratory on pure products at a temperature of 20°C in fresh water. These controlled conditions are quite different from those encountered in case of a real incident at sea. In addition, the SEBC also fails to provide any information on the physico-chemical processes explaining the observed mixed behaviour, their kinetics and their eventual competitions. As a consequence, further experimental characterization of chemicals behaviour at different scales (ranging from laboratory to the field) is needed in order to gain a better understanding of the physico-chemical processes at stake, to develop more reliable mathematical models of these processes (taking into account the actual environmental conditions) and eventually to provide more accurate answers to decision makers when they plan response efforts and pollution control.

1.4 HNS-MS objectives

The project HNS-MS aimed at developing a decision-support system that national maritime authorities and coastguard stations can activate to forecast the drift, fate and behaviour of acute marine pollution by Harmful Noxious Substances (HNS) accidentally released in the marine environment.

Focussing on the Greater North Sea and Bay of Biscay, this 2 year project (01/01/2015-31/03/2016) had four specific objectives:

i. To develop a freely accessible data base documenting the most important HNS transported from or to the ports of Antwerp, Rotterdam, Hamburg, Nantes and Bordeaux;
ii. To conduct lab experiments in order to improve the understanding of the physico-chemical behaviour of HNS spilt at sea;
iii. To develop a 3D mathematical modelling system that can forecast the drift, fate and (SEBC) behaviours of HNS spilt at sea. Advanced processes such chemical reactivity, explosions, fire or interaction with sediment were not considered in this first project;
iv. To produce environmental and socioeconomic vulnerability maps dedicated to HNS that will help end-users assessing the likely impacts of HNS pollution on the marine environment, human health, marine life, coastal or offshore amenities and other legitimate uses of the sea.

All these contributions have been integrated into a web application that will help coastguard stations to evaluate the risks for maritime safety, civil protection and marine environment in case of acute pollution at sea.

1.5 HNS-MS workflow

To meet HNS-Ms objectives, the workflow has been subdivided into 10 tasks articulated around 4 main axes (Figure 2):

1. **Lab experiments:** The first axis aims at collating or producing data and information to support the development of the HNS drift and fate model. First a selection of 100+ important HNS transported in the Bonn Agreement area has been performed from a literature and database review. Then, keeping in mind that only processes fully understood can accurately be simulated; several laboratory experiments have be carried out in order to improve our understanding of HNS behaviour both in the water column and at the sea surface. For instance, for the first time, a Lab experiment has been conducted in order to quantify the competition between the evaporation and dissolution kinetics of chemical floating at the sea surface. Finally, two field campaigns have been organised.

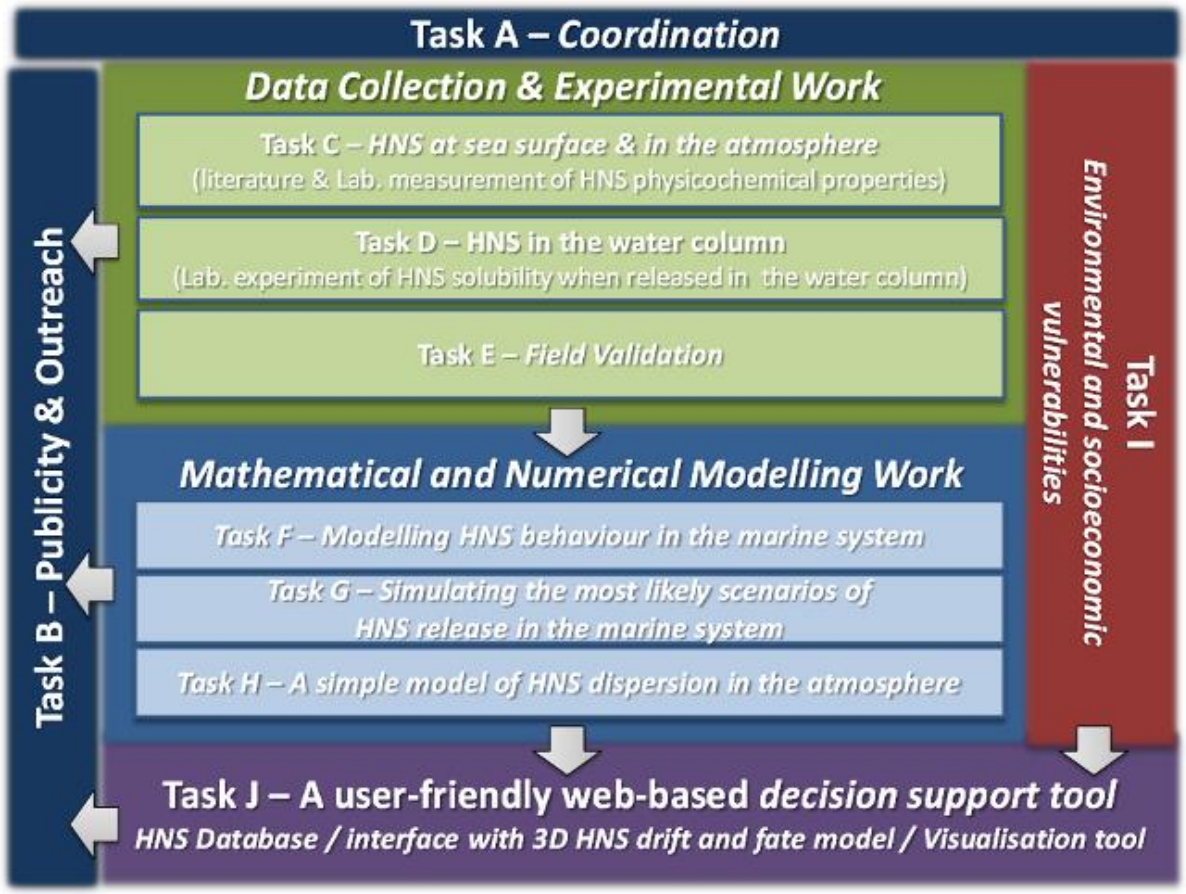

Figure 2: HNS-MS workflow is articulated around 4 main axes: Lab experiments, model development, environmental and socio-economic vulnerabilities mapping and development of a Decision Support System. (Figure from the project proposal submitted to DG-ECHO call to projects 2014)

2. **Mathematical modelling:** The second axis aims at developing a 3D HNS drift and fate modelling software. In order to handle (i) the large variety of HNS physico-chemical properties, (ii) the large variety of possible spillage scenarios and (iii) the large variety of the involved time and space scales, three different models have been developed, namely
    - ChemSPELL, HNS-MS near-field model
    - ChemDRIFT, HNS-MS far-field model
    - ChemADEL, HNS-MS atmospheric dispersion model
3. **Environmental and socio-economic vulnerabilities:** The third axis aims at developing a series of regional and local vulnerability for HNS-sensitive environmental and socioeconomic features. The HNS-MS vulnerability ranking methodology is mainly an extension of methodology developed in the framework of the BE-AWARE projects, also funded by DG-ECHO.

4. **Decision support System:** Finally, the fourth axis aims at integrating all the previously obtained results in an intuitive, easy-to-use operational web-based HNS decision-support system for the Bonn Agreement area and the Bay of Biscay.

1.6 Why a new model of the drift, behaviour and fate of HNS spills at sea?

According to a recent survey (Bonn agreement, 2016), 16 different operational oil spills drift and fate models are routinely used by the Bonn Agreement contracting parties (Figure 3, left). If 5 of these modelling systems are implementations of a commercial software (OILMAP or OSCAR), the 11 other models are in-house or public models operated by the different national agencies involved in operational oceanography and marine forecasting. In view of the scientific expertise available the latter national agencies, it can be reasonably assumed that the end-users of the oil drift and fate model predictions can also receive an adequate support to understand what are the strengths, weaknesses, limitations and uncertainties of the modelling system, leading to correct interpretation of the model results.

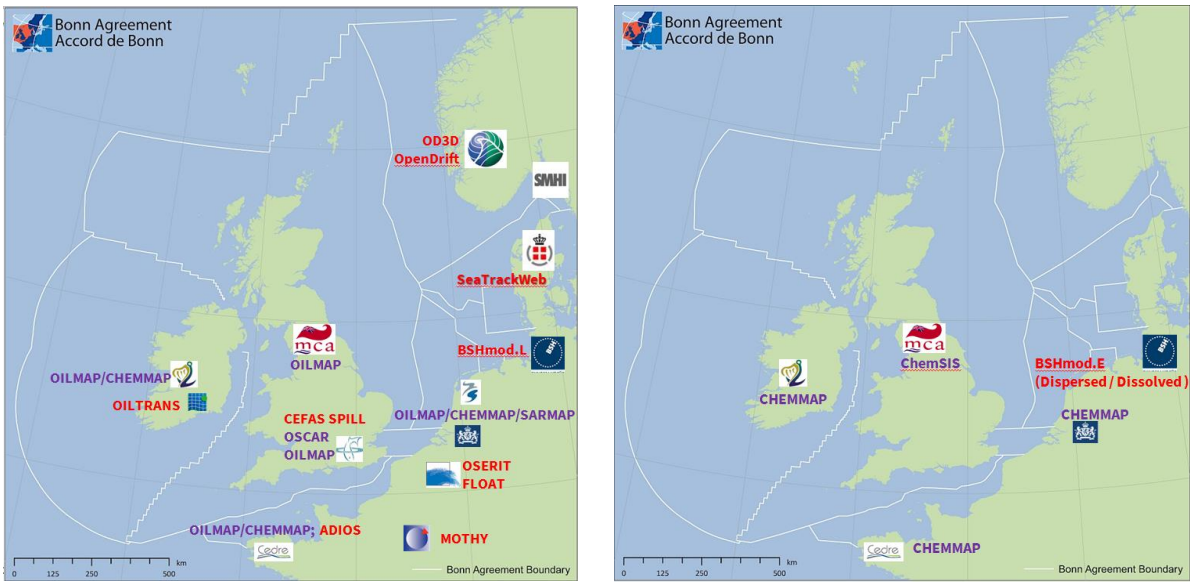

Figure 3: While oil spill drift and fate models (left) are common tools in the Bonn Agreement area, only a few contracting parties operate HNS spills drift , behaviour and fate models (right). In red : in-house or open source model; in purple : commercial solutions. (Bonn Agreement, 2016)

According the same survey, the situation is totally different for the HNS spills drift, behaviour and fate models: only 5 different systems are routinely operated by the Bonn Agreement contracting parties, out of which three are implementation of the same commercial solution CHEMMAP, one is an implementation of the deprecated commercial solution CHEMSIS and the last one is BSH's in-house advection-diffusion model for dissolved substances (Figure 3, right).

The objective of the HNS-MS consortium is therefore to develop a new state-of-the-art in-house HNS drift, behaviour and fate model whose developers and maintainers can have a full control on the various implemented modules, algorithms and products and whose operators and end-

users can have a fair enough understanding of its strengths, weaknesses, limitations and uncertainties to make correct interpretation of its results.

1.7 Challenges and simplifications

The purpose of the HNS-MS model is to predict the drift, behaviour and fate of harmful and noxious chemical substances spilt in the marine environment for the first hours and days after the spillage in the greater North Sea (also known as the Bonn Agreement area), its Atlantic margin and the Bay of Biscay. This model is intended to help maritime authorities and decision-makers assessing the likely impact of a HNS acute maritime pollution event on the marine environment, human health, marine life, coastal or offshore amenities and other legitimate uses of the sea and therefore the model will help planning the most efficient response strategy.

Developing such a model is a threefold challenge because of

i. The wide variety of the HNS products (a.o. liquids, solids, gas – in bulk or packaged) and their wide range of physico-chemical properties;

ii. The wide variety of HNS behaviours at sea involving numerous physico-chemical processes spanning time and space scales ranging from tenths of second to years and from millimetres to hundreds or thousands of kilometres ;

iii. The wide variety of possible accidents and spill release conditions (leaking tank, adverse weather leading to unstable cargo / ship, loss of containers, collisions, capsizing, hull damage, grounding, sinking, danger of fire, explosion, chemical reaction in cargo, …).

The development of a model that tackles all these issues in a suitable way will surely remain a long lasting research topic for the coming decade(s). In this relatively short (2-year) project, several acceptable simplifications had to be made.

The first main simplification consisted in restricting our developments to the case of ***pure HNS transported in bulk***. Focussing on pure HNS allowed us to not consider complex processes occurring with HNS mixtures such as weathering and chemical reactions. We have not considered neither self-reaction processes nor polymerisation processes as e.g. occurred with styrene spilt from the "Ievoli Sun" wreck sunk off Britany (France) on 31/10/2000. Eventually, as the case of the MSC-Flaminia perfectly illustrated in 2012, HNS mixtures mainly raises concerns for packaged HNS shipped in containers or drums so that we could reasonably focus our developments to the case of HNS transported in bulk.

The second simplification consisted in not trying to model "instantaneous" violent event and their consequences such as chemical explosion (including combustion and fire) or physical

explosion[3]. However, although the HNS-MS modelling system is not meant to predict the risk of explosion, the end-users of the HNS-MS decision support system (cf. sub-report IV) may there find key information as flash point or lower and upper explosive limits for HNS presenting a risk of explosion.

Finally, the third main simplification consisted in not considering the interaction between HNS and sediments, neither in the water column nor at the seabed. However, these interactions might have some effect on the fate of HNS spilt in coastal and estuarine turbid areas, such as for instance the Belgian part of the North Sea.

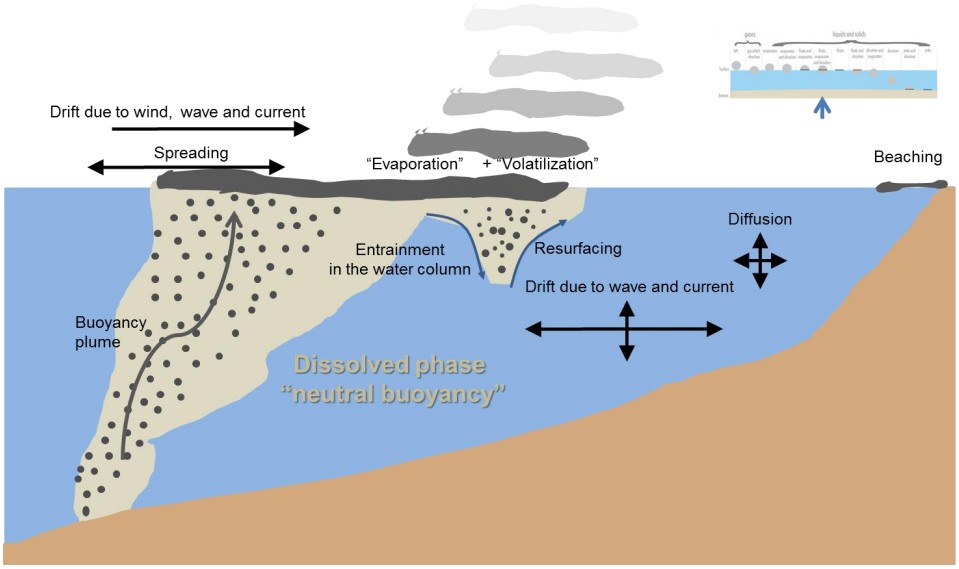

Figure 4: The main physico-chemical processes influencing the drift, fate and behaviour of a Floater-Evaporator-Dissolver liquid HNS - case of a spillage from a subsurface source.

1.8 HNS-MS modelling strategy

Taking into account the 3 main simplifications presented in the previous section, our objective was to develop a state-of-the-art modelling system able to simulate the physico-chemical processes explaining the 4 main SEBC behaviours. As illustrated in Figure 4 for the case of a Floater-Evaporator-Dissolver, these processes are various and includes drift (advection) due to current, waves and wind, dilution due to turbulent mixing, vertical (upward or downward) slip

[3] Also known as rapid phase transition explosion, a physical explosion is realised when a liquefied gas (as LNG, shipped at temperature of - 160°C) violently vaporises upon coming in contact with seawater (about 15°C). This results in an explosion because the volume occupied by natural gas in its gaseous phase is 600 times greater than the volume occupied by the liquefied gas. Usually, these explosions projects at very high speed tiny ice crystals and microscopic cold water droplets that can cause serious injuries.

velocity due to buoyancy, resurfacing, natural entrainment in the water column due to surface agitation (waves), beaching, sinking to the seabed, evaporation, volatilisation...

The exact list of the processes **simultaneously** acting on the drift, behaviour and fate of HNS maritime pollution depends on the physical state of the pollutant, its physico-chemical properties and the environmental conditions. The list of processes taken into account in HNS-MS modelling strategy as well as some underlying hypothesis are summarized Table 1, Table 2 and Table 3, for gaseous, liquid and (raw) granular solid HNS respectively.

Following the example of RBINS state-of-the-art 3D oil spill drift and fate model OSERIT, all these processes have been model using a Lagrangian particle tracking approach. According to this method, a pollution event is represented by a cloud of particles to which is associated a fraction of the pollutant volume. At each model timestep, the model computes the new position of the particles as well as the repartition of the pollutant mass associated between the different possible physical states in function of the processes taken into account.

Actually, because the different processes can still involve a wide range of time and space scales, 3 different but linked models have been developed in the framework of the project:

1. ChemSPELL, as a near-field model, mainly aiming at modelling processes occurring at small time and space scales, from a few seconds to an hour and from a few meters to a few kilometres away from the source.
2. ChemDRIFT, as a far-field model, mainly aiming at modelling processes occurring at larger time and space scales, from hours to a week and from a few hundreds of meters to tens or hundreds of kilometres away from the source
3. ChemADEL, as a Gaussian puff atmospheric dispersion model.

The full details of these models are presented in chapters 3, 4 and 5, respectively.

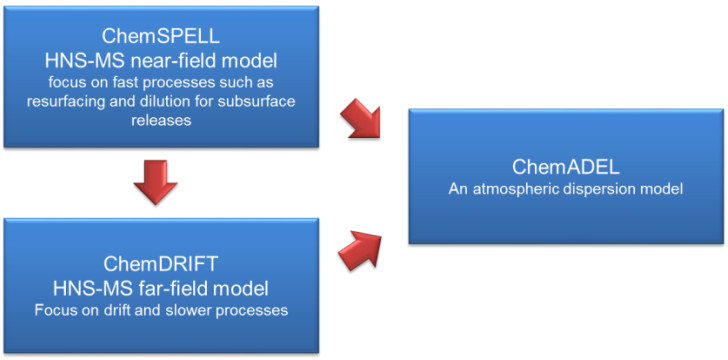

Figure 5: Three different models have been implemented as a function of time and space scales of the process involved. The red arrows show how model results of one model can feed the initial conditions of another model.

Table 1: Processes taken into account in HNS-MS modelling strategy in order to simulate the drift, behaviour and fate of gaseous HNS maritime pollution

Gaseous HNS	Physical state	SEBC class	Processes
Air	Gas cloud	Evaporator Gas	• Advection of the gas cloud due to wind • Dilution / dispersion of the gas cloud as a function of the atmospheric stability and distance from the source
Sea Surface	Gas bubble	Gas	• All the gas bubbles released from a surface source reaching the sea surface instantaneously goes in the air. However, knowing the location of the resurfacing is an information of interest for responders.
Water column	Gas bubble	G and GD	• Dissolution (GD only) • Rising slip velocity, function of and bubbles' size and buoyancy • Advection-diffusion due to subsurface current, waves and turbulence mixing • Turbulent jet (plume dynamic stage) near subsurface source under pressure.

Table 2: Processes taken into account in HNS-MS modelling strategy in order to simulate the drift, behaviour and fate of liquid HNS maritime pollution

Liquid HNS	Physical state	SEBC classes	Processes
Air	Gas cloud	Evaporator	• Advection of the gas cloud due to wind • Dilution / dispersion of the gas cloud as a function of the atmospheric stability and distance from the source
Sea Surface	Surface slick	Floater, Evaporator, Dissolver	• Drift to current, wind and waves (Stokes drift). • Surface slick spreading • Entrainment in the water column due to sea surface agitation (waves) or HNS density –> formation of HNS droplets • [Evaporator only] Evaporation in the air as a function of the the HNS vapour pressure, HNS temperature, air temperature and wind • [Dissolver only] Dissolution in the water column as a function of HNS solubility and viscosity, concentration of the dissolved fraction in the water column and the surface of the slick
Water column	droplets	Floater, sinker, dissolver	• Drift due to subsurface current and waves (subsurface stokes drift) • Rising [Floater] or falling [sinker] slip velocity as a function of and droplets' size and buoyancy • Turbulent jet (plume dynamic stage) near subsurface source under pressure. • [Floater only] Resurfacing : droplets reaching the sea surface, contributing again to the surface slick. • [Dissolver only] Dissolution in the water column as a function of HNS solubility and viscosity, concentration of the dissolved fraction in the water column and the droplets diameter • [sinker only] droplets reaching the seabed can "sediment" to the seabed to form a slick covering the seabed
Water column	Dissolved fraction	Dissolver only	• Drift due to subsurface current and waves (subsurface stokes drift) • No rising or falling slip velocity because the dissolved fraction is assumed to be at the same density as the surrounding sea-water • Volatilisation of the dissolved fraction in contact with sea surface as a function of the HNS vapour pressure and limit of solubilitty
Seabed	Slick covering the seabed	Sinker and dissolver	• No resuspension or bedload transport • [Dissolver only] Dissolution in the water column as a function of HNS solubility and viscosity, concentration of the dissolved fraction in the water column and the surface of the slick

Table 3: Processes taken into account in HNS-MS modelling strategy in order to simulate the drift, behaviour and fate of maritime pollution by granular solid HNS or powder

Granular solid and powder	Physical state	SEBC classes	Processes
Air	Gas cloud	Evaporator	• Advection of the gas cloud due to wind • Dilution / dispersion of the gas cloud as a function of the atmospheric stability and distance from the source
Sea Surface	Solid grain	Floater, Evaporator, Dissolver	• Drift to current, wind and waves (Stokes drift). • Spreading due to wave agitation and turbulent mixing • Entrainment in the water column due to sea surface agitation (waves) or grain density [grain size remains unchanged] • [Evaporator only] Evaporation in the air as a function of the the HNS vapour pressure, HNS temperature, air temperature and wind • [Dissolver only] Dissolution in the water column as a function of HNS solubility and viscosity, concentration of the dissolved fraction in the water column and grain size
Water column	Solid grain	Floater, sinker, dissolver	• Drift due to subsurface current and waves (subsurface stokes drift) • Rising [Floater] or falling [sinker] slip velocity as a function of and droplets' size and buoyancy • Turbulent jet (plume dynamic stage) near subsurface source under pressure. • [Floater only] Resurfacing of all grains reaching the sea surface. • [Dissolver only] Dissolution in the water column as a function of HNS solubility and viscosity, concentration of the dissolved fraction in the water column and grain size • [sinker only] droplets reaching the seabed can "sediment" to the seabed to form a "slick" covering the seabed
Water column	Dissolved fraction	Dissolver	• Drift due to subsurface current and waves (subsurface stokes drift) • No rising or falling slip velocity because the dissolved fraction is assumed to be at the same density as the surrounding sea-water • [if evaporator] Volatilisation of the dissolved fraction in contact with sea surface as a function of the HNS vapour pressure and limit of solubilitty
Seabed	Slick covering the seabed	Sinker and dissolver	• No resuspension or bedload transport • [Dissolver only] Dissolution in the water column as a function of HNS solubility and viscosity, concentration of the dissolved fraction in the water column and the surface of the slick

1.9 Release scenarios

There exist a large variety of possible maritime accident and HNS spillage conditions, including leaking tank, adverse weather conditions leading to unstable cargo / ship, loss of containers, collisions, capsizing, hull damage, grounding, sinking, danger of fire, explosion, chemical reactions in cargo...

To be useful, our modelling system must be able to handle the widest possible range of spillage conditions, also called **model initial conditions** in modellers' jargon. Because ChemSPELL, ChemDRIFT and ChemADEL are all based on (different flavours of) the Lagrangian particles techniques, imposing initial model conditions is equivalent to impose to **each** Lagrangian particle

- A release time (aka start time);
- A release location (longitude, latitude) and depth. The also includes a tag if at sea surface, in the water column, at the seabed or in the air;
- Its initial momentum (usually negligible);
- The physico-chemical properties of the associated HNS;
- A fraction of the total HNS volume released at sea (usually but not necessary the total volume divided per the number of Lagrangian particle);
- The distribution of this volume per possible physical state (usually one).

Because a simulation typically requests tens or hundreds of thousands of Lagrangian particles, manually encoding the initial conditions quickly becomes a tedious task. This is the reason why we have predefined 9 likely release scenarios for which initial conditions are automatically computed:

1. **Observed pollution at sea surface**
    a) Small to medium slick (Surface slick as a circle or an ellipsis)
    b) Elongated slick (Pollution as a straight line)
2. **Pollution in the water column** (Pollution as an extruded ellipsis)
3. **Pollution of the sea floor** (Pollution covers an ellipsis area)
4. **Release from a moving vessel** (Pollution along a straight line)
5. **Release from a leaking wreck**
    a) Discharge rate estimated
    b) Discharge rate computed
6. **Spill from a broken pipeline**
7. **Release from a land source or a river**
8. **Direct gas release in the atmosphere**

9. Release from leaking containers adrift

Selecting the right release scenarios is equivalent to answering the question

"How is HNS spilt in the marine environment?"

Once the scenario is selected, the model operator will then have to answer the 3 questions

"What [is released]?"
"When [does the spillage occur]?"
"Where [does the spillage take place]?"

The exact formulation of these questions depends on the selected scenario and it is thought that their answers should be quite straightforward, providing some coarse estimation or common sense (some default values are also suggested). There is however one exception: the estimation of the discharge rate and the draining time in case of a slow leak from a sunken wreck (scenario 5b). In this case, a specific model has been developed to compute the discharge rate as a function of the leaking tank characteristic and the breach(es) size and location. This model, presented in chapter 0, is intended to be used in case of a long-lasting pollution.

1.10 Metocean forcing

Environmental conditions are an important external factor that drives or influences the drift, behaviour and fate of HNS maritime pollution. Otherwise stated, the accuracy of the metocean forcing will determine the accuracy and reliability of the HNS-MS model simulation results.

The HNS-MS domain of interest covers the whole greater North Sea, its Atlantic margin and the Bay of Biscay. Currently, the most accurate ocean data source covering the whole area are the physical forecast produced by monitoring and forecasting centre of the North West European Continental Shelf (MFC-NWS) from the Copernicus Marine Environment Monitoring Service (CMEMS – http://marine.copernicus.eu/). Formally known as "NORTHWESTSHELF_ANALYSIS_FORECAST_PHYS_004_001_b", this product provides analysis and 6 day forecast of sea surface elevation, 3D-hourly gridded ocean current, temperature and salinity fields for the area covering 20°W to 13°E and 40°N to 65°N with an horizontal resolution of ~7km (1/9° lon X 1/15° lat). 3D fields are provided at 25 depths: 0m, 3m, 10m, 10m, 15m, 20m, 30m, 50m, 75m, 100m, 125m, 150m, 200m, 250m, 300m, 400m, 500m, 600m, 750m, 1000m, 1500m, 2000m, 3000m, 4000m, 5000. Information on the product and its

quality can be found in the "Product User Manual"[4] and the "Quality Information Document"[5] and the references within.

Because CMEMS does not provide weather and waves forecast for the same area, ECMWF's hourly atmospheric and waves forecast are re-interpolated on the NWS grid.

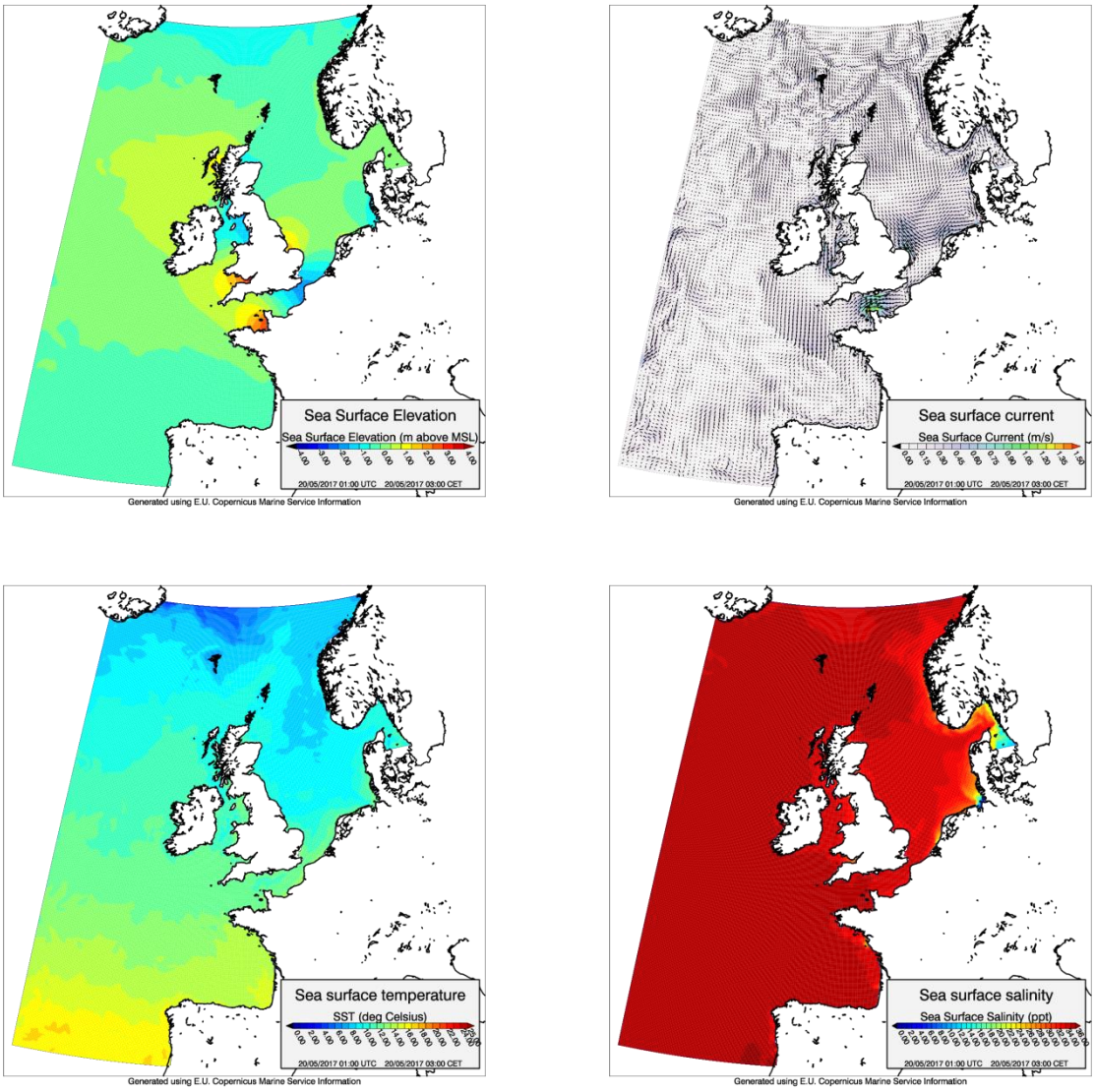

Figure 6: Snapshot of sea-surface elevation, currents, temperature and salinity forcing.
Source: CMEMS' Atlantic - European North West Shelf - Ocean Physics Analysis and Forecast.

[4] http://marine.copernicus.eu/documents/PUM/CMEMS-NWS-PUM-004-001.pdf
[5] http://marine.copernicus.eu/documents/QUID/CMEMS-NWS-QUID-004-001-002.pdf

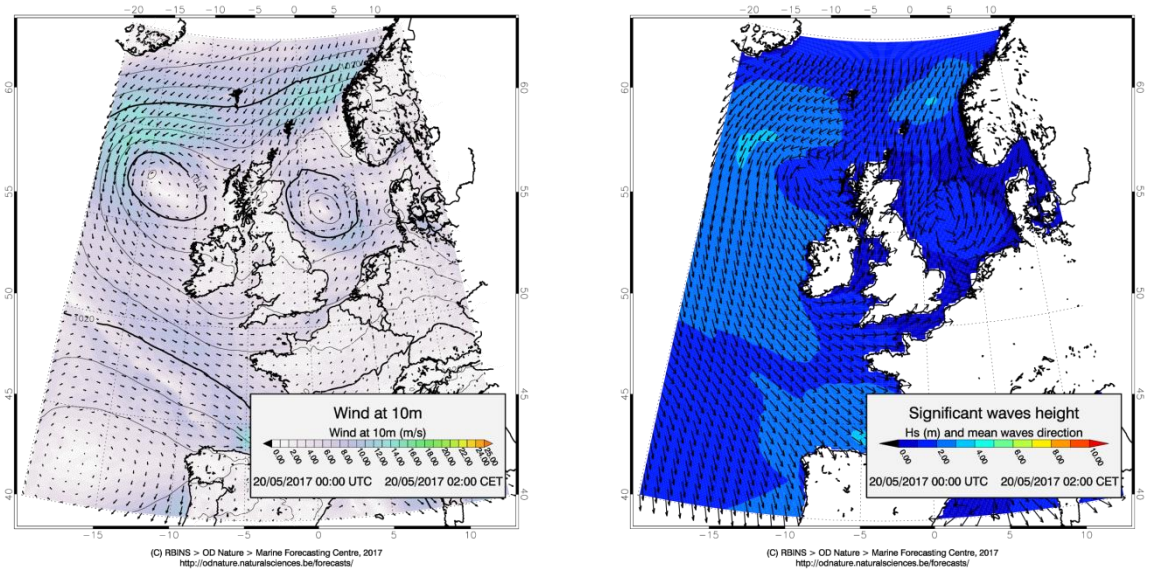

Figure 7: Snapshot of atmospheric and waves forcing.
Source : ECMWF NWP forecast re-interpolated on CMEMS grid.

Spillage from a leaking wreck

PAGE INTENTIONALLY LEFT BLANK

2 Spillage from a leaking wreck

2.1 Introduction

The increase in maritime transport generates highly frequented zones between the world's major ports as English Channel and North Sea. The combination of these narrow areas with the high density traffic inevitably increases the risk of accidental spills with serious environmental and human damage. The Channel concentrates 20 % of global traffic and is a necessary passage for ship vessels linking the Atlantic Ocean to the North Sea. Every day, 700 to 800 vessels pass through the Strait of Calais and potentially dangerous cargoes (oil, chemicals, containers ...) is increasing. The number of chemicals transported in bulk rised from 30 Mt/y in 1988 to 150 Mt/y in 2000. Neuparh identifies many accidents due to the important traffic in this narrow area with 86 accidents occurred in the Channel and 70 % involved oil spills between 1960 and 2007 (Neuparh et al., 2012). Moreover, the number of accidents decreases although the volume transported is increasing since 1985. This decrease can be attribute to the improvement of the security transportation (Bahé, 2008). However, since 1990, the number of accidents with chemicals increases and involves new risks (explosion, toxic releases…). The Ievoli Sun sank about 16.7 km from north Casquets by 70 m of depth with chemicals including 3998 tons of styrene, 1 027 t of methyl ethyl ketone (MEK) and 996 t of isopropyl alcohol (IPA) (Law et al., 2003). In addition, the ship contained propulsion fuel (160 t of Intermediate Fuel Oil (IFO) and 220 t of diesel). The release quantities from vessel were 400 t of Styrene (Figure 8), 100 t of MEK and 996 t of IPA. This wreck is not the only example of a chemical loss, in 2001 the Balu sank with 8000 t of sulfuric acid in the Bay of Biscay at 4,600 m of depth; in 2006, the Ece discharged 10,000 t of phosphoric acid by 70 m deep. The improvement of the risks management for a tanker accident requires the evaluation of consequences at short term for the rescue teams and at long terms to determine the impact on humans and marine environment (Neuparh et al., 2011). To derive this, the different quantities of dissolved, floating and evaporating parts are required and depends on the physico-chemical parameters of the chemical release, on the marine and weather forecasts (streams, temperature, wind …) and on other variables as the spill volumic flow rates, distribution of droplets size or the rising velocity of chemicals. It noticed that many studies exist on spill modelling at different scales.

Figure 8: Styrene release following the Ievoli Sun wreckage observed by French Navy

When a ship sinks with a breach both in the hull and in a cargo tank containing floating chemicals, leakage causes an ascending plume of substances toward the surface (Figure 9). The release of a floating liquid from a vessel aground on the seabed generally corresponds to a release without injection speed and depends only on the fluid properties. The release rate, hydrodynamics and dissolution rate of the chemicals are issues which should be considered to assess the volume of product reaching the surface.

To achieve this action, experimental tests were performed in the ECUD (Experimental Column for Underwater Discharge) to simulate underwater HNS release. This document presents the experimental results and the conclusion to model the underwater discharge.

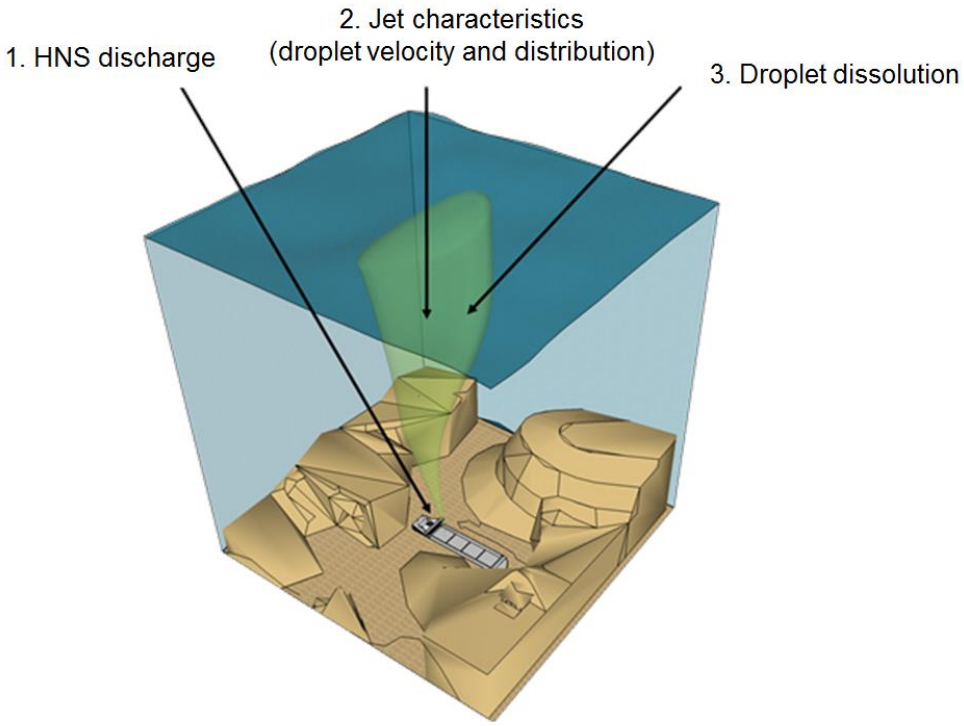

Figure 9: Illustration of shipwreck and chemical release from seabed

2.2 Underwater discharge theory

Transportation tanks in ships are large parallelepipeds up to 10 meters high. Figure 10 represents the blue print of the Ievoli Sun. The largest tank capacity (in red) at a capacity of 630 m^3 (L x W x H: 12 x 7.5 x 7 m). Considering a gaseous phase of 30 cm of height, the volume is about 600 m^3 of product. The filling level is variable. Although it is preferable to fill up the tanks to avoid any sloshing effect and to stabilize the ship at sea, a gaseous headspace is inevitable. Whatever the ship position on the seafloor after wreckage, the initial configuration is a gaseous space above the commodity volume (Figure 11). It has to be noticed that some sea-water will enter the perforated tank during the sink of the ship due to pressure variation. Moreover, in the case of shipwreck on seabed, the gas volume in the tank is adjusted to compensate the hydrostatic pressure due to high water column above the ship.

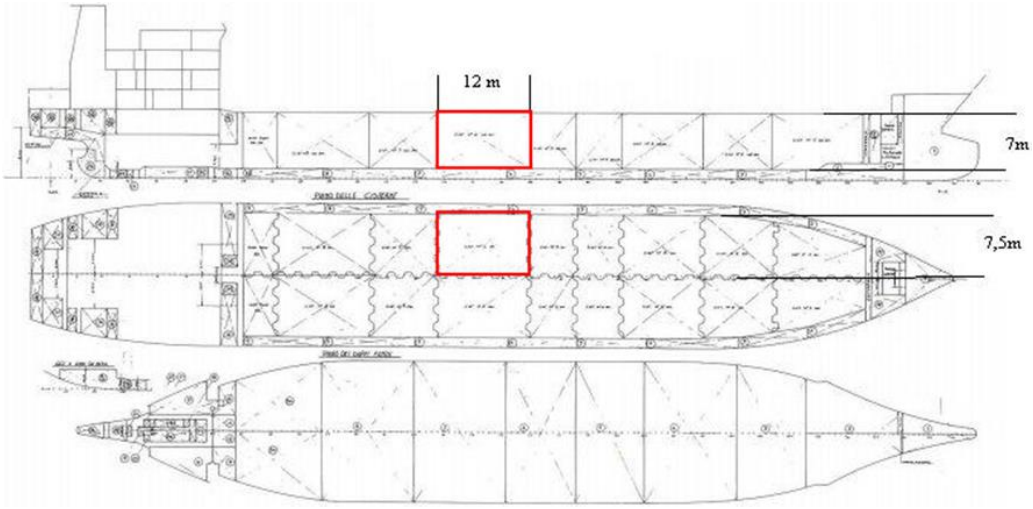

Figure 10: Blue print of Ievoli Sun chemical tanker (Beamer, 2001)

2.2.1 Floating chemicals behaviour

Let us assume a ship containing chemicals lighter than sea-water with an opening (break) below the waterline, from where the chemical leaks into the sea. This problem is governed by unsteady outflow/inflow driven by gravity. The hydrostatic pressure difference across the break due to density difference between fluids is the key factor to analyse the leak rate.

In case of a single breach, different configurations can be considered:

- The breach is located at a top position (Figure 11, case A, arrow 1), the gas will be entirely released and replaced with water creating a layer under the chemical (case B).
- The breach is located below the top but still at gas level (situation A, arrow 2) some gas will be trapped in a cavity which should be considered as a dead space and therefore excluded from the study of discharge (case C);
- The breach is located at the chemical level (situation A, arrow 3), causing its release. The ejected volume is replaced by an equivalent volume of water. This situation will continue until the position D is reached. Both gas and chemical will remain trapped in the tank in a dead space.

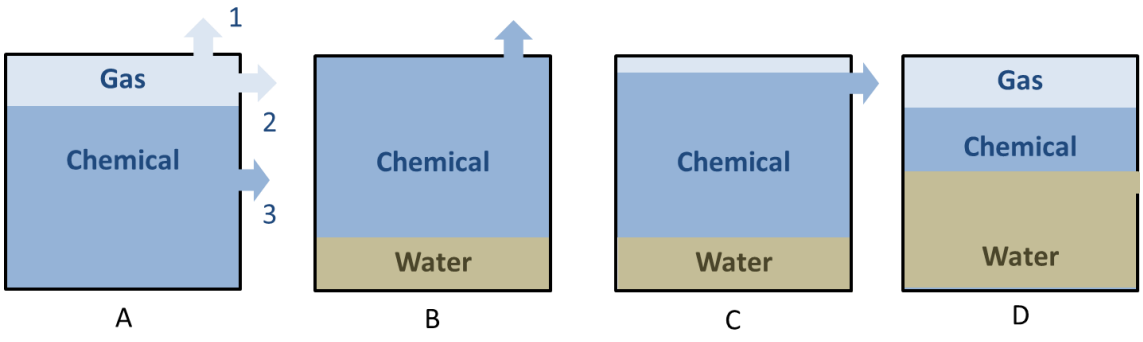

Figure 11: Influence of the breach location in case of a single hole for floating product

It is also possible that the ship damage entailed two or more breaches, or an initial single breach made the ship sink and another breach was created when the wreck reached the seabed (Figure 12). Two different behaviours have to be noticed, depending on the position of the breaches (case E and case F).

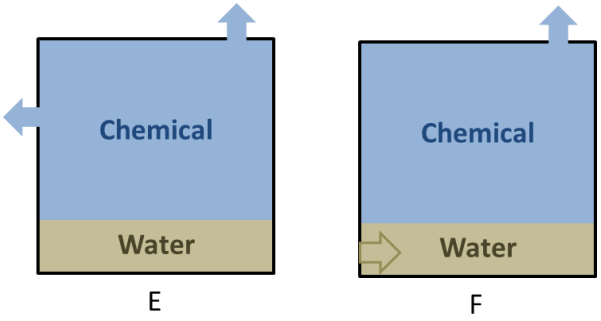

Figure 12: Influence of the breach location in case of multiple holes for floating product

The leak will stop when the water level reaches the upper orifice. In all cases, determining how many chemical will remain in the tank after the end of leakage will therefore require getting (by submarine investigation for example) the orifice location and ship position on the seafloor.

2.2.1.1 Modelling of draining vessel filled with floating chemicals

The vessel is considered as an open system exchanging substance and energy with the outside (Figure 13). From a conceptual point of view, the position and number of holes does not matter.

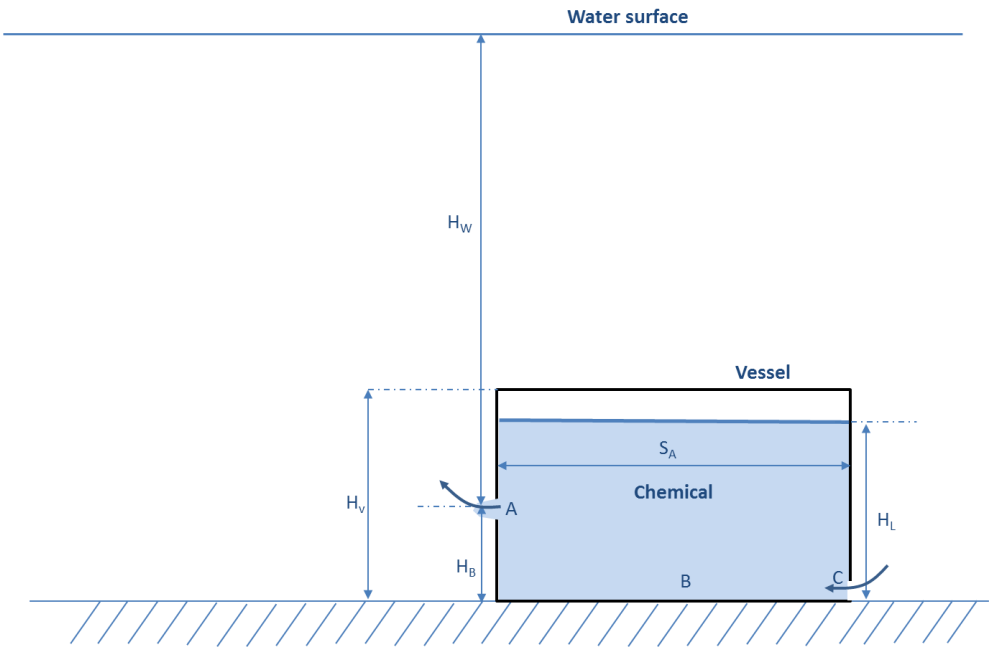

Figure 13: Illustration of draining phenomena for floating chemical released from submerged vessel with two breaches.

Some assumptions are necessary to define the problem:

The fluids will be assumed incompressible, the static pressure at initial time (t=0) is then written:

$$P_A = P_{atm} + \rho_W g H_W$$
$$P_B = P_A + \rho_L g H_B \quad (1)$$
$$P_C = P_A + \rho_w g H_B$$

Where P_{atm} is the atmospheric pressure (Pa), H_w the height of water column above the breach (m), ρ_W the density of sea-water (kg.m^{-3}), ρ_L the density of the chemical phase (kg.m^{-3}); The heights H_L corresponds to the initial height of chemical phase in the vessel (m), H_V the total height of vessel (m) and H_B the height of the breach (m) from bottom of the vessel.

The volume flow conservation Q (kg.m^{-3}) is defined as:

$$Q = A_B U_A = S_B U_B = S_C U_C \quad (2)$$

Where S_A, S_B, S_C are respectively, the section of chemical outflow (m^2), the horizontal vessel section (m^2), the section of water inflow (m^2). U_A, U_B et U_C are respectively the fluid velocity (m.s^{-1}) at the breach level, at the horizontal vessel section and at the inlet water flow section. It is noticed the size of the breach is lower than the horizontal vessel section, then:

$$S_A \ll S_B$$
$$U_A \gg U_B \quad (3)$$

The system is defined only during the draining time T(s). The system the following equations are defined for any time t(s) as:

$$0 < t \leq T \; with \; Q(T) = 0 \quad (4)$$

2.2.1.2 Flow rate modelling

2.2.1.2.1 The case of double breach

The draining vessel is calculated with the Bernoulli principle derived from the principle of conservation of energy. This requires that the sum of kinetic energy, potential energy and internal energy remains along a streamline of a perfect fluid:

$$E_C + E_P + P = cst \quad (5)$$

with:

- E_C : Kinetic energy per unit volume : $E_C = \frac{1}{2}\rho U^{*2}$
- E_P : Potential energy per unit volume : $E_P = \rho g z$
- P : Pressure energy

The exponent symbol * represents the perfect fluids velocities

The application of the Bernoulli principle on a streamline from B to A in the chemical phase leads to:

$$P_{atm} + \rho_w g(H_W + H_B) - \rho_L g H_B + \frac{1}{2}\rho_L U_B^{*2} = P_{atm} + \rho_w g H_W + \frac{1}{2}\rho_L U_A^{*2} \quad (6)$$

Simplifying Eq. (6)

$$g H_B - \rho_L g + \frac{1}{2}\rho_L U_B^{*2} = \frac{1}{2}\rho_L U_A^{*2} \quad (7)$$

Then,

$$(\rho_w - \rho_L) g H_B + \frac{1}{2}\rho_L U_B^{*2} = \frac{1}{2}\rho_L U_A^{*2} \quad (8)$$

Using the assumption (3), the initial chemical velocity at breach is given by :

$$U_A^* = \sqrt{2 g H_B \frac{(\rho_w - \rho_L)}{\rho_L}} \quad (9)$$

In the present study, fluids are not perfect, the Bernoulli relationship has to be modified to take into account the energy losses due to friction by a constant parameter called velocity coefficient. In addition, at breach level, the chemical jet will contract until the current lines can be considered as straight and parallel (Figure 14). In this zone, called the *vena contracta*, the section S_C of the chemical outflow is smaller than the breach section S_B. These diameters are linked by the contraction coefficient.

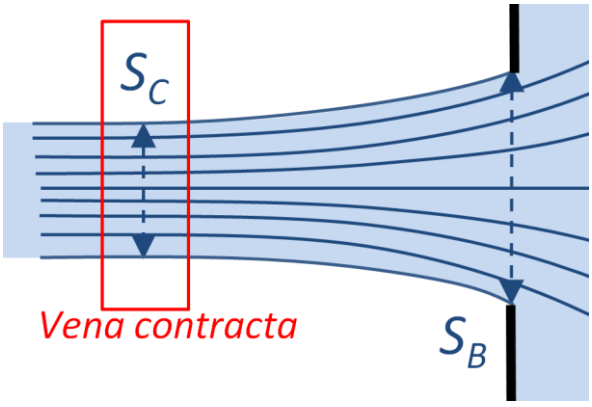

Figure 14: Illustration of the vena contracta for chemical release at breach level.

The product of velocity coefficient and contraction coefficient defines the discharge coefficient C_D. The value of the discharge coefficient depends on the geometry and orientation of the breach. The values reported by Dodge et al. (1980) range from 0.577 to 0.629 for inward edges at the breach, and from 0.622 to 0.828 for outward edges. During marine accident, the

evaluation of breach shape is not being easier; it is proposed to use the mean value of discharge coefficient:

$$C_D = 0.703 \tag{10}$$

The correction of the chemical velocity V_A^* by discharge coefficient C_D leads to:

$$U_A = C_D U_A^* \tag{11}$$

Then, the real chemical velocity at breach level can be obtained by the following equation:

$$U_A = C_D \sqrt{2gH_B \frac{(\rho_w - \rho_L)}{\rho_L}} \tag{12}$$

$$U_A = 0.703 \sqrt{2gH_B \frac{(\rho_w - \rho_L)}{\rho_L}} \tag{13}$$

2.2.1.2.2 The case of single breach

As mentioned in the paragraph 2.2.1, in the case of single breach the chemical and the sea-water are flowing through the same orifice as illustrated by the Figure 15. Then the chemical velocity at breach level is modified to take into account the decrease of the flow section (Figure 16). Figure 16 represents the DEHA flow through a round orifice of 30mm diameter during single breach experiment. The figure clearly shows the low flow section area for the chemical. It is noticed the experimental measurements of chemical section at breach level is tricky and requires new experimental tests with adapted optical measurements devices. However, it has been observed that chemical cross section at breach level was in a range between 20% to 50% of the total breach section.

Then, it is proposed to calculate the real chemical velocity release for single breach configuration with a correction factor of 35% corresponding to an estimation of the real cross section of the chemical flow:

$$U_A = 0.35 C_D \sqrt{2gH_B \frac{(\rho_w - \rho_L)}{\rho_L}} \tag{14}$$

$$U_A = 0.246 \sqrt{2gH_B \frac{(\rho_w - \rho_L)}{\rho_L}} \tag{15}$$

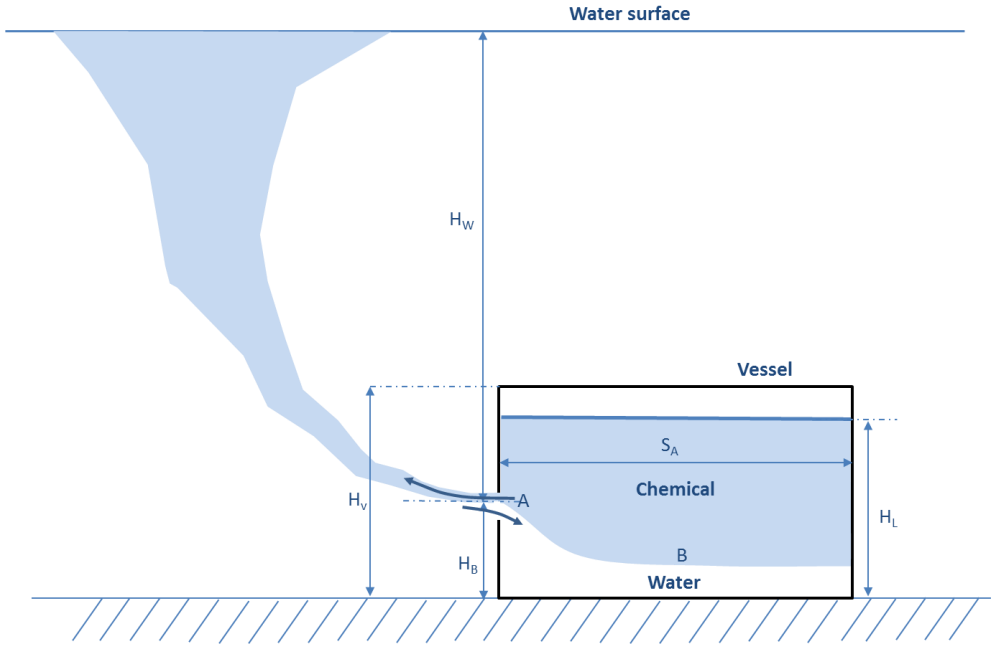

Figure 15: Illustration of draining phenomena for floating chemical released from submerged vessel with single breach.

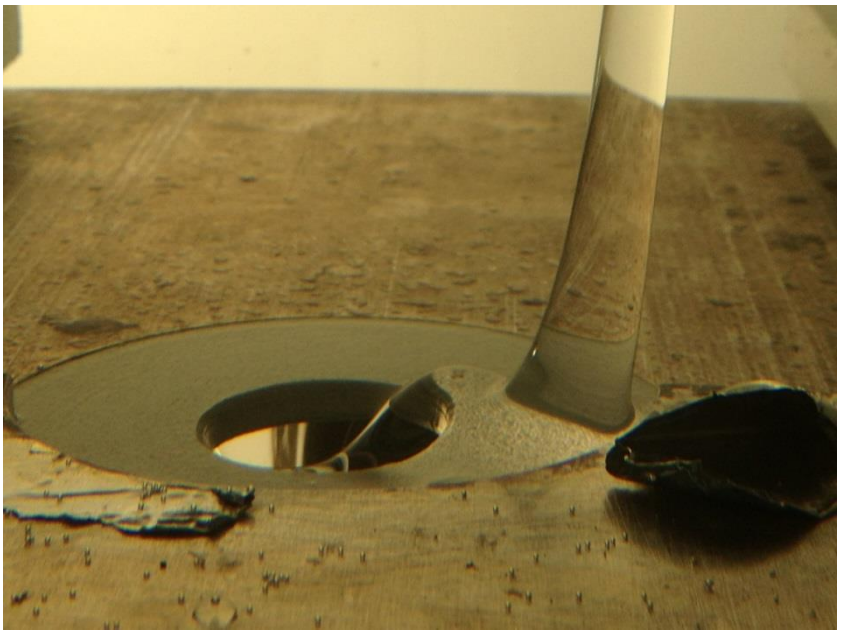

Figure 16: Illustration of the decrease of cross section flow for DEHA released in sea-water.

2.2.2 Sinking chemicals behaviour

In the same manner as the behavior of chemicals lighter than sea-water, a submerged ship draining chemicals heavier than sea-water is characterised by unsteady outflow/inflow driven by gravity and by the density difference between fluids.

To characterize leak at the breach and vessel draining, two configurations are considered:

- The breach is located at a top position (Figure 17, case A, arrow 1), the gas will be entirely released and replaced with water creating a layer above the chemical (case B).
- The breach is located on the side in the chemical phase (situation A, arrow 2) Phase gas is trapped in a cavity which should be considered as a dead space and therefore excluded from the study of discharge (case C). This situation will continue until the position D is reached. It is noticed that chemical will remain trapped in the tank in a dead space below the breach.

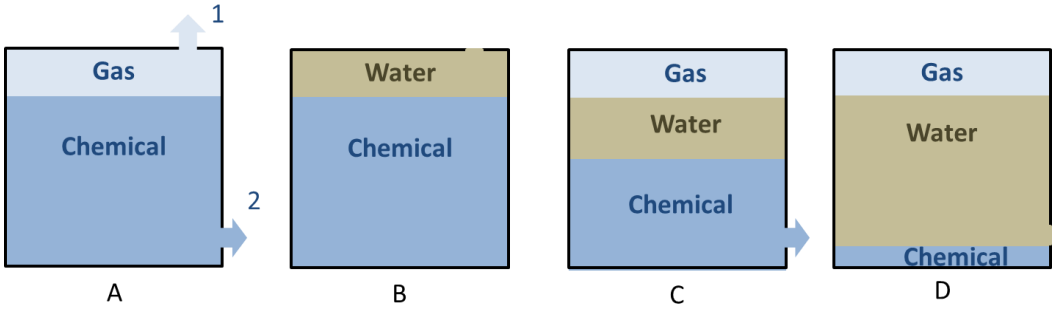

Figure 17: Influence of the breach location in case of a single hole for sinking product

It is also possible that the ship damage entailed two or more breaches, or an initial single breach made the ship sink and another breach was created when the wreck reached the seabed (Figure 18). Two different behaviours have to be noticed, depending on the position of the breaches (case E and case F).

- The first breach is located in the gas phase and the second breach in the chemical (case E). Gas is entirely release and replaced by water. Chemical is flowing by the second breach until water level reaches the bottom of the breach.
- In the case F, gas is trapped in the dead space, water flow inside the vessel and chemical flow outside until water level reaches the bottom of the breach.

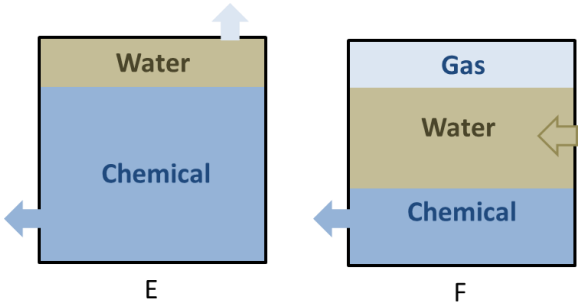

Figure 18: Influence of the breach location in case of multiple holes for sinking product

As for floating product, the determination of draining vessel requires how many chemical will remain in the tank after the end of leakage and then, the orifice location and ship position on the seafloor.

2.2.2.1 Modelling of draining vessel filled with sinking chemicals

In the same manner as for floating product, the draining vessel for sinking product is calculated with the Bernoulli principle. The assumptions propose in the paragraph 2.2.1.1 are also valid for sinking products. Figure 19 illustrates the draining of vessel with two breaks and filled with sinking chemical.

The application of the Bernoulli principle on a streamline from B to A in the chemical phase leads to:

$$P_{atm} + \rho_w g\big(H_W - (H_L - H_B)\big) + \rho_L g(H_L - H_B) + \frac{1}{2}\rho_L U_B^{*2} = P_{atm} + \rho_w g H_W + \frac{1}{2}\rho_L U_A^{*2} \quad (16)$$

Simplifying Eq. (16)

$$\rho_L g(H_L - H_B) - \rho_w g(H_L - H_B) + \frac{1}{2}\rho_L U_B^{*2} = \frac{1}{2}\rho_L U_A^{*2} \quad (17)$$

Then,

$$(\rho_L - \rho_W) g(H_L - H_B) + \frac{1}{2}\rho_L U_B^{*2} = \frac{1}{2}\rho_L U_A^{*2} \quad (18)$$

Using the assumption (3) $U_A \gg U_B$, the initial chemical velocity at breach is given by:

$$U_A^* = \sqrt{2g(H_L - H_B)\frac{(\rho_L - \rho_W)}{\rho_L}} \quad (19)$$

The chemical real velocity is then obtained using the discharge coefficient C_D:

$$U_A = C_D\sqrt{2g(H_L - H_B)\frac{(\rho_L - \rho_W)}{\rho_L}} \quad (20)$$

$$U_A = 0.703\sqrt{2g(H_L - H_B)\frac{(\rho_L - \rho_W)}{\rho_L}} \quad (21)$$

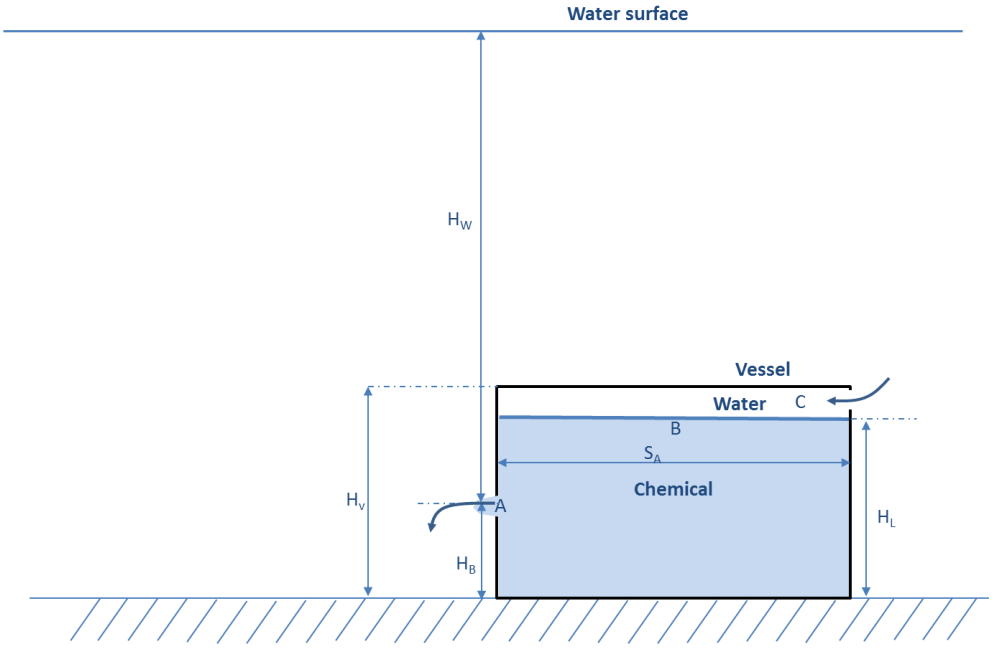

Figure 19: Illustration of draining phenomena for sinking chemical released from submerged vessel with two breaches

For vessel with 2 orifices (Figure 20), the approach is the same as for floating products and leads to use the same correction factor of 35%.

$$U_A = 0.35.C_D\sqrt{2g(H_L - H_B)\frac{(\rho_L - \rho_W)}{\rho_L}} \quad (22)$$

$$U_A = 0.246\sqrt{2g(H_L - H_B)\frac{(\rho_L - \rho_W)}{\rho_L}} \quad (23)$$

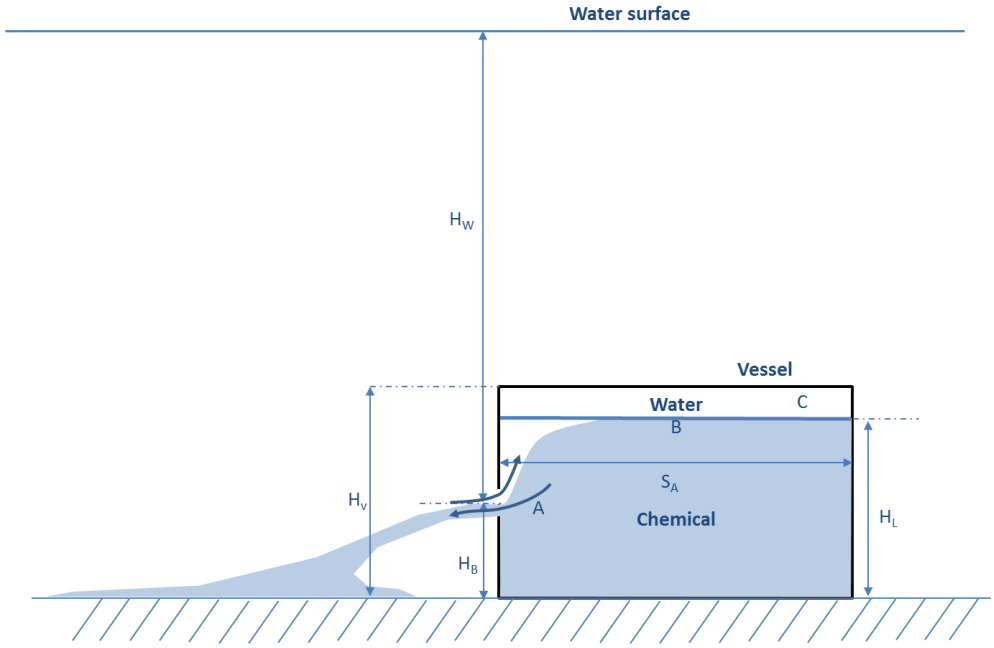

Figure 20: Illustration of draining phenomena for sinking chemical released from submerged vessel with single breach

2.2.3 Modelling strategy

The following steps explain the strategy to calculate the draining of submerged chemical vessel. We assume there is not gas phase in the vessel and, the leak stop above (for floating product) or below (for sinking product) the breach.

A. Intel parameters

- Chemical density (kg m^{-3}): ρ_L
- Sea-water density (kg m^{-3}): ρ_W
- Chemical height in the vessel (m): H_L
- Breach high (m): H_B
- Breach size (m) : D_B (m) or L_B, l_B
- Vessel size (m): L_V, l_V, H_V

B. Intermediate calculations

- Hydraulic diameter $D_H(m)$
  - Circular break: $D_H = D_B$
  - Longitudinal breach: $D_H = 2.\frac{L_B.l_B}{L_B+l_B}$

- Total chemical volume released (m^3): V_L
  - Floating product: $V_L = L_V.l_V.H_B$
  - Sinking product: $V_L = L_V.l_V.(H_L - H_B)$

- Initial chemical velocity at breach (m.s^{-1}): U_A
  - Floating product:
    - 1 breach : $U_A = 0.703\sqrt{2gH_B\frac{(\rho_W-\rho_L)}{\rho_L}}$
    - 2 breaches : $U_A = 0.246\sqrt{2gH_B\frac{(\rho_W-\rho_L)}{\rho_L}}$
  - Sinking product:
    - 1 breach : $U_A = 0.703\sqrt{2g(H_L-H_B)\frac{(\rho_L-\rho_W)}{\rho_L}}$
    - 2 breaches : $U_A = 0.246\sqrt{2g(H_L-H_B)\frac{(\rho_L-\rho_W)}{\rho_L}}$

C. Draining calculation at each time step ΔT(s)

- Floating product:
  - Chemical volume released (m³): $V_{LR}(t_n) = U_A(t_n).\pi.\left(\frac{D_H}{2}\right)^2.\Delta t$
  - Chemical volume remaining in the vessel (m³): $V_{RL}(t_n) = V_{RL}(t_{n-1}) - V_{LR}(t_n)$
  - Chemical height remaining in the vessel (m): $H_{RL}(t_n) = \frac{V_L(t_n)}{L_V.l_V}$
  - Chemical velocity at breach (m.s^{-1}):

$$U_A(t_{n+1}) = 0.703\sqrt{2g\left(H_B - H_{RL}(t_n)\right)\frac{(\rho_W-\rho_L)}{\rho_L}}\ \text{(1 breach)}$$

$$U_A(t_{n+1}) = 0.246\sqrt{2g\left(H_B - H_{RL}(t_n)\right)\frac{(\rho_W-\rho_L)}{\rho_L}}\ \text{(2 breaches)}$$

- Sinking product:
  - Chemical volume released (m³): $V_{LR}(t_n) = U_A(t_n).\pi.\left(\frac{D_H}{2}\right)^2.\Delta t$
  - Chemical volume remaining in the vessel (m³): $V_{RL}(t_n) = V_{RL}(t_{n-1}) - V_{LR}(t_n)$
  - Chemical height remaining in the vessel (m): $H_{RL}(t_n) = \frac{V_L(t_n)}{L_V.l_V}$
  - Chemical velocity at breach:

$$U_A(t_{n+1}) = 0.703\sqrt{2g(H_{RL}(t_n) - H_B)\frac{(\rho_L-\rho_W)}{\rho_L}}\ \text{(1 breach)}$$

$$U_A(t_{n+1}) = 0.246\sqrt{2g(H_{RL}(t_n) - H_B)\frac{(\rho_L-\rho_W)}{\rho_L}}\ \text{(2 breaches)}$$

2.2.4 Tests case

2.2.4.1 Floating product

A. Inlet parameters

- Chemical density: 930 kg.m^{-3}
- Sea-water density: 1030 kg.m^{-3}
- Vessel characteristics:
  - L_V=12 m

- l_V=7.5 m
- H_V=6.65 m

- Breach characteristics:
  - D_B=0.2 m
  - H_B=4 m

B. Results

- Draining time :
  - 1 breach: 531 min
  - 2 breaches: 184 min
- Total volume released: $V_{TR} = L_V . l_V . (H_B + D_B) = 378$ m³

2.2.4.2 Sinking product

A. Inlet parameters

- Chemical density: 1130 kg.m^{-3}
- Sea-water density: 1030 kg.m^{-3}
- Vessel characteristics:
  - L_V=12 m
  - l_V=7.5 m
  - H_V=6.65 m
- Breach characteristics:
  - D_B=0.2 m
    H_B=4 m

B. Results

- Draining time :
  - 1 breach: 476 min
  - 2 breaches: 165 min
- Total volume released: $V_{TR} = L_V . l_V . H_B = 238.5$ m³

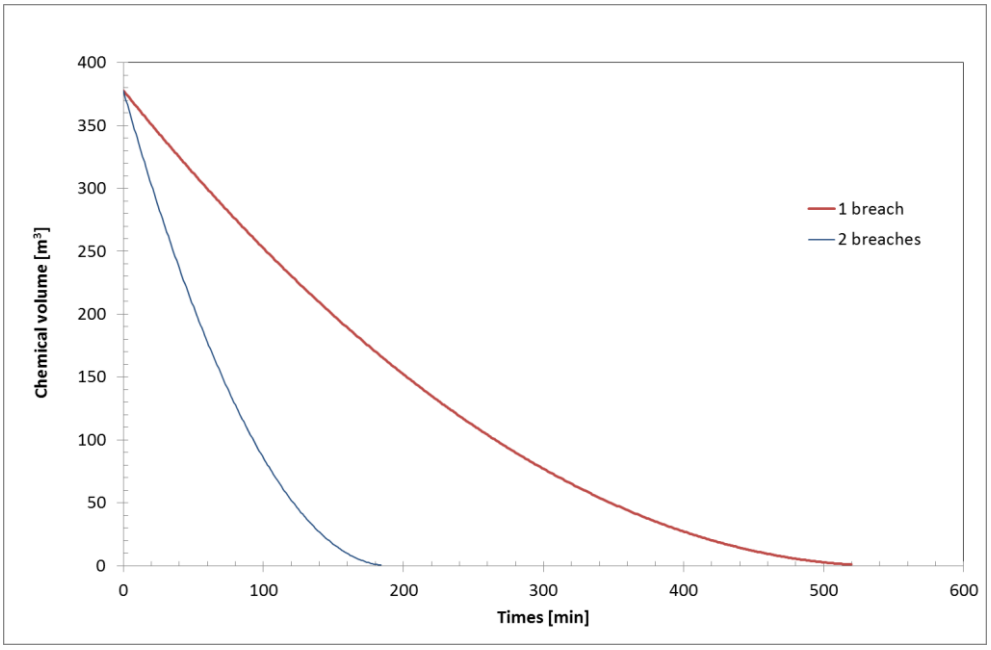

Figure 21: Draining time for floating product

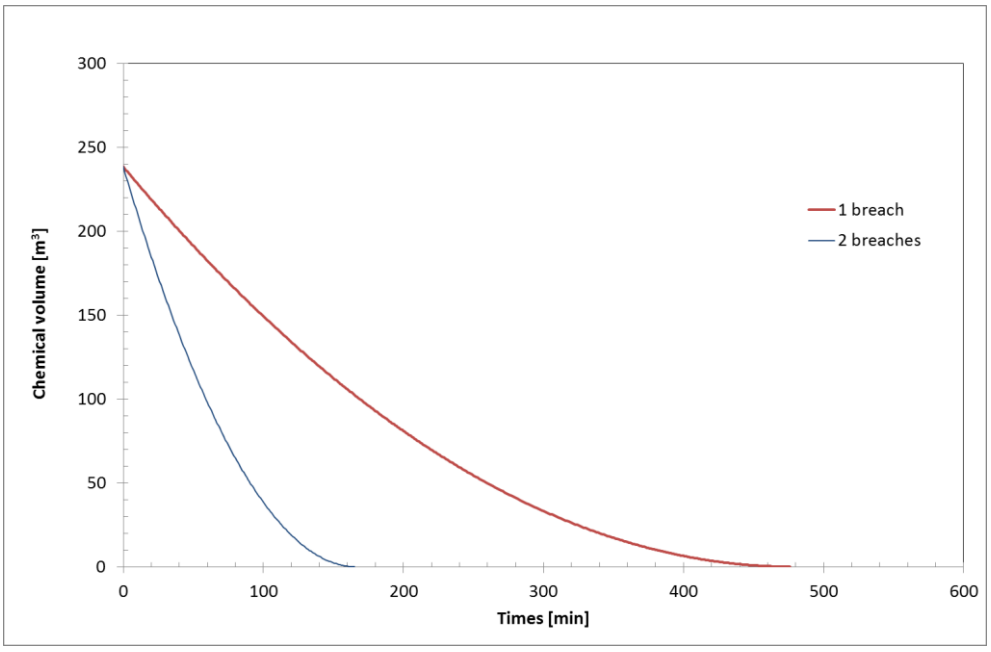

Figure 22: Draining time for sinking product

ChemSPELL
HNS-MS near field model

PAGE INTENTIONALLY LEFT BLANK

3 ChemSPELL, HNS-MS near-field model

3.1 Introduction

In the scope of the HNS-MS project, Improving Member States preparedness to face an HNS pollution of the Marine System, ALYOTECH has developed a near-field model for underwater release scenario of chemical including blowout from wells or pipeline, and leakage from sunken vessels. In addition to the need of covering various release scenarios, it appears necessary to cover the likely behaviour in the water column, according to the Standard European Behaviour Classification (SEBC). Then the present model can deal with the five category (floaters, sinkers, gases, evaporators and dissolvers) and combinations of them, taking into account the physical and chemical properties of the product.

A special attention is done on the dissolution phenomena because of the environmental impact, as dissolvers can be a source of potential of toxicity for the marine environment. Thus dissolved mass of chemical has to be quantified precisely. Dissolution is implemented in a dedicated module used in ChemSPELL, and callable by HNS-MS far-field model.

The purpose of the present chapter is to present the mathematical models from the literature as well as models elaborated from experiments done in task D.1 and D.2, both used in the ChemSPELL (Chemical Subsea Plume modEL for Leakage) code.

3.2 Mathematical models

In ChemSPELL, the HNS release is treated in two different transport stages (Figure 23). An initial stage deals with the first part of the plume, i.e. close to the surface, where hydrodynamics are governed by the momentum and the mixing inside the plume, a result from the ambient water entrainment into the plume. Then the plume reaches a neutral buoyancy level (NBL), corresponding to the end of the plume dynamics: Momentum is negligible and the passive advection and diffusion behaviour becomes the dominant process to transport the substance. The HNS will rise as parcels of numerous droplets/bubbles, following the ambient current and rising due to their own buoyancy.

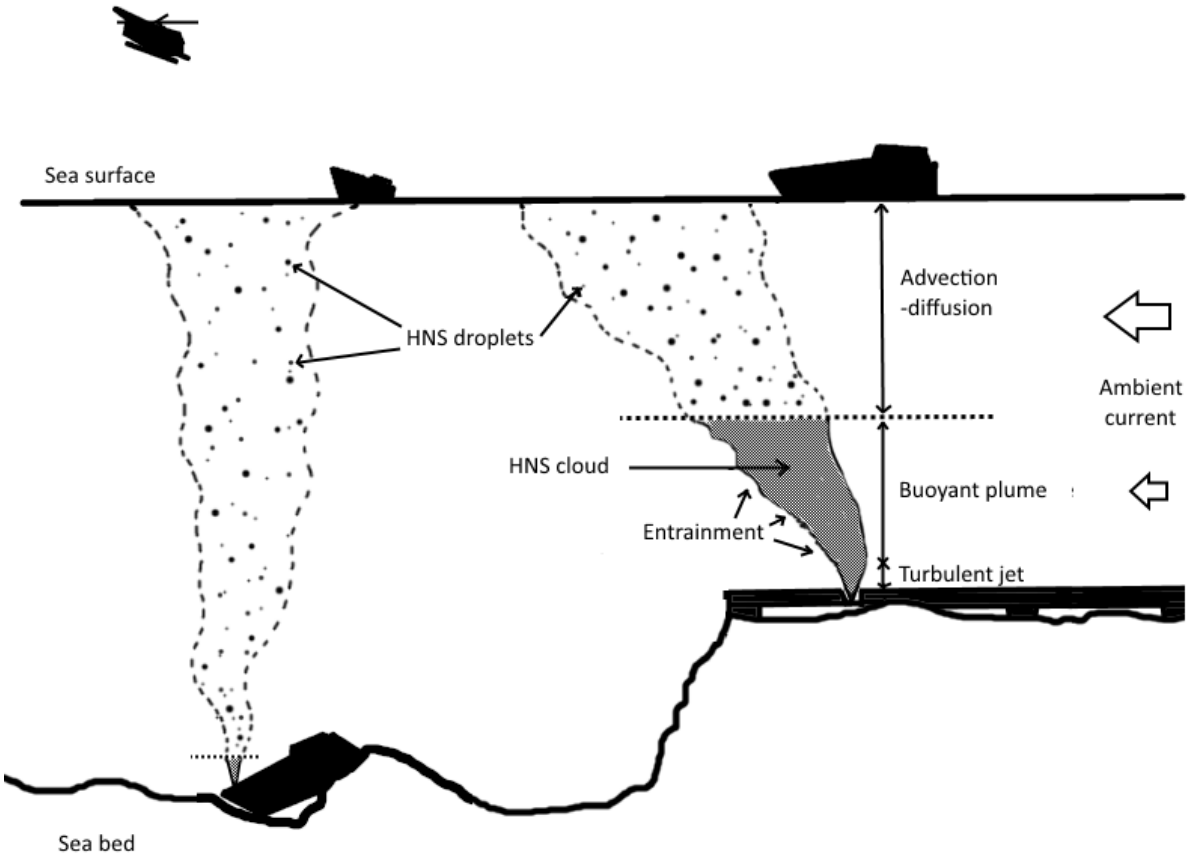

Figure 23 : Illustration of HNS leaks in the water column (Alyotech, 2016)

3.2.1 Model initialization

The flow rate modelling for sunken vessels in ChemSPELL is based on the **Error! Reference source not found.** chapter, for the different configurations of a submerged tank with simple or double breach, and for both floating and sinking pollutant. In all cases, the Bernoulli principle is

used and adapted to evaluate the velocity. Table 4 presents the different formulas implemented in the sunken vessel scenario in ChemSPELL.

	Simple breach	Double breach
Floating HNS	$U_a = 0.703\sqrt{2gH_B\frac{(\rho_w-\rho_L)}{\rho_L}}$	$U_a = 0.246\sqrt{2gH_B\frac{(\rho_w-\rho_L)}{\rho_L}}$
Sinking HNS	$U_a = 0.703\sqrt{2g(H_L-H_B)\frac{(\rho_L-\rho_w)}{\rho_L}}$	$U_a = 0.246\sqrt{2g(H_L-H_B)\frac{(\rho_L-\rho_w)}{\rho_L}}$

Table 4 : Summary of initial velocity evaluation for a sunken vessel (Aprin, 2016)

The model needs also the description of the droplet size distribution as input of the Plume Dynamics Stage (PDS). The work done in task D.2, and reported in the technical report for HNS-MS "*Characterization of the HNS behaviour in the water column*" (Aprin 2016), provides that information. The droplet distribution is based on normal distribution with a probability distribution function as:

$$f(d) = \frac{1}{d\,\sigma\sqrt{2\pi}}\,e^{-\frac{1}{2}\left(\frac{\ln(d)-\mu}{\sigma}\right)^2} \qquad (24)$$

In which σ and μ are the mean and standard deviation of the variable's natural logarithm. Experiments have been conducted on releases of di ethyl exyl adipate (DEHA). The report underlines the fact that the distribution is linked to the flow rate: it can be mono-modal or bi-modal. The Table 5 summarizes the coefficients from experiments.

	$Q < 10^{-4}m^3s^{-1}$		$Q \geq 10^{-4}m^3s^{-1}$
μ	-5.69	-4.51	-5.3
σ	0.561	0.364	0.635

Table 5 : Summary of log-normal law parameters, adapted to the distribution from experiments (Aprin, 2016)

The modelling law described above is implemented in ChemSPELL, and its use is extended for all chemicals.

In the cases of well and pipeline scenarios, the volumic flow rate is given as an input parameter, so the source term is directly used as initial conditions. The released pollutant temperature is also an input parameter as it influences solubility in case of gas.

Moreover two additional parameters are required in the case of pipeline release, θ and ϕ, corresponding to the break orientation: ϕ is the angle between the jet trajectory and the horizontal plane (rad^{-1}), and θ the angle between the x-axis and the projection of the jet

trajectory on the horizontal plane (rad^{-1}) (Figure 24). In shallow water, the break orientation for a pipeline can have a major effect on the location of the surfacing plume.

For those two scenarios of large release, none information on the HNS droplet size distribution has been found in the literature. By default, the "high" flow droplet size distribution from the sunken vessel scenario is selected.

3.2.2 Plume dynamic stage

The jet-plume part is based on a Lagrangian model (Lee and Cheung, 1990; Yapa, 1997), in which a control volume is tracked as it moves along the centreline of the buoyant jet with its local centreline velocity $\mathbf{v}$ (m/s). The evolution of its properties, radius b (m), thickness $h = \mathbf{v}\Delta t$ (m), and mass $m = \rho\pi b^2 h$ (kg) is tracked over time.

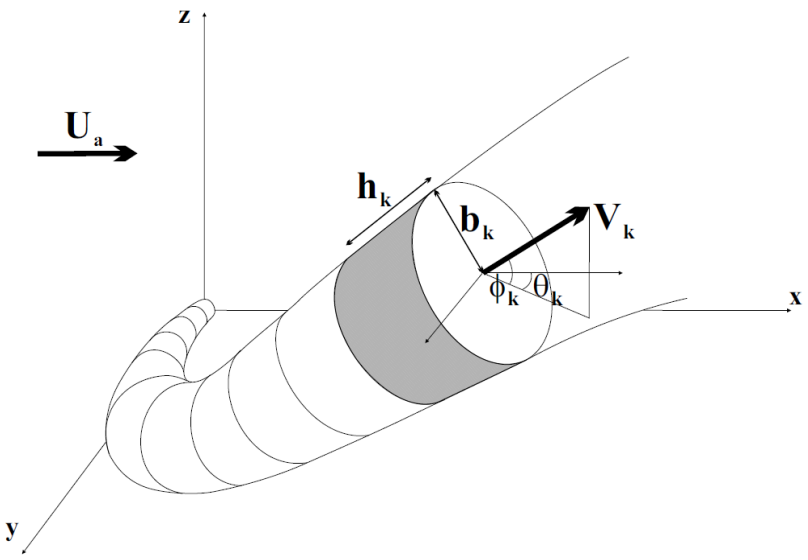

Figure 24 : Schematic diagram of jet trajectory traced out by Lagrangian plume elements from the 3D lagrangian model for buoyant jet (Lee, 1990)

The mass variation in the plume is linked to the volume flux Q_e (m^3/s) oriented towards the inner structure and entrained by the turbulent eddies. The fluid in the control volume is considered as a mixture of water and chemical forming a single phase with density ρ (kg/m^3). The conservation of the liquid mass m_l is:

$$\frac{dm_l}{dt} = \rho_a Q_e - \frac{dm_d}{dt} \qquad (25)$$

where ρ_a is the density of ambient water (kg.m^{-3}), $\frac{dm_d}{dt}$ the dissolution rate of the pollutant entity (mol.s^{-1}). The volume flux Q_e is the result of the shear-induced entrainment between the

buoyant jet and the water Q_s ($m^3.s^{-1}$), and a forced entrainment due to the advection of current into the buoyant jet Q_v ($m^3.s^{-1}$):

$$Q_s = 2\pi bh\alpha \left| |\vec{V}| - V_a' \right| \quad (26)$$

with V_a' the ambient water current velocity magnitude ($m.s^{-1}$), and α an entrainment coefficient such as:

$$\alpha = \sqrt{2}\frac{0.057 + \frac{0.554 \sin\varphi}{F^2}}{1 + 5\frac{V_a'}{\left| |\vec{V}| - V_a' \right|}} \quad (27)$$

and

$$F = E\frac{\left| |\vec{V}| - V_a' \right|}{\left(g\frac{\Delta\rho}{\rho_a} b \right)^{1/2}} \quad (28)$$

in which ϕ an angle between the jet trajectory and the horizontal plane, E a proportionality constant, taken here to 2. The forced entrainment components of Q_v are evaluated as follow:

$$\begin{cases} Q_{vx} = \rho_a |u_a| \left[\pi b \Delta b |cos\theta cos\phi| + 2b\Delta s\sqrt{1 - cos^2\theta cos^2\phi} + \frac{\pi b^2}{2} |\Delta(cos\theta cos\phi)| \right] \\ Q_{vy} = \rho_a |v_a| \left[\pi b \Delta b |sin\theta cos\phi| + 2b\Delta s\sqrt{1 - sin^2\theta cos^2\phi} + \frac{\pi b^2}{2} |\Delta(sin\theta cos\phi)| \right] \\ Q_{vz} = \rho_a |w_a| \left[\pi b \Delta b |sin\phi| + 2b\Delta s |cos\phi| + \frac{\pi b^2}{2} |\Delta(sin\phi)| \right] \end{cases} \quad (29)$$

with (u_a, v_a, w_a) the ambient velocity V_a' components ($m.s^{-1}$), and θ the angle between the x-axis and the projection of the jet trajectory on the horizontal plane. The second term of the right-hand of (25) side represents the dissolution of liquid HNS into water, and is treated in the Dissolution model section.

The momentum equations are applied to the average within the control volume. The drag force is neglected. The momentum equations can be written as follows:

$$\frac{d}{dt}(m_l \mathbf{V}) = \mathbf{V}_a \rho_a Q_e + \mathbf{k} m_l \frac{(\rho_a - \rho_l)}{\rho_l} g \quad (30)$$

where $\mathbf{v}_a$ is the velocity of the ambient environment (m/s) and a unit vector $\mathbf{k}$ in the vertical direction. State variables like heat, salinity, concentration are also considered, following:

$$\frac{d}{dt}[m_l T_{pl}] = T_a \rho_a Q_e \quad (31)$$

$$\frac{d}{dt}[m_l S_{pl}] = S_a \rho_a Q_e \quad (32)$$

$$\frac{d}{dt}[m_l C_{pl}] = C_a \rho_a Q_e$$

where T_{pl} and T_a respectively the temperature of the plume and of the ambient water (K); S_{pl} and S_a the salinity of the plume and of the ambient water (PSU). C_{pl} and C_a the concentration of the pollutant in the plume and of the ambient water (kg/m^3).

In a gaseous HNS release context, liquid and gas mass conservation equation in the control volume change to:

$$\frac{dm_l}{dt} = \rho_a Q_e \quad (33)$$

$$\frac{dm_g}{dt} = -\frac{Nh}{w + w_s}\frac{dm_d}{dt} \quad (34)$$

The first right hand side in the conservation of gas mass is the number of bubbles per unit plume height. The flux of the number of bubbles N .(s^{-1}) is considered constant with height (coalescence is neglected). w_s here is the slip velocity of a gas bubble (m/s).

Moreover, additional terms have to be taken into account in momentum conservation equation (30) in order to consider the presence of gas:

$$\frac{d}{dt}((m_l + m_g)\mathbf{V} + \mathbf{k} w_s m_g) = \mathbf{V}_a \rho_a Q_e + \mathbf{V} \rho_g Q_g + \ldots \quad (35)$$
$$\mathbf{k}\left[(\rho_a - \rho_l) g \pi b^2 (1 - \beta\varepsilon h) - (\rho_a - \rho_g) g \pi b^2 \beta\varepsilon h\right]$$

where ρ_g and Q_g represent respectively the gas density (kg/m^3) and the gas volume flux (m^3/s). ε is the void fraction of gas in the control volume such as $\varepsilon = \frac{\rho_l - \rho}{\rho_l - \rho_g}$. The continuous phase (liquid) and dispersed phase (bubbles) are treated as a single mixture with density ρ (kg/m^3).

3.2.3 Advection-diffusion stage

As the plume moves upwards, it loses momentum and buoyancy due to entrainment of ambient water. The plume dynamics are no longer high. Then beyond this depth, the HNS undergoes advection-diffusion combined with its own buoyant velocity (Dasanayaka, 2009). The pollutant is divided into a large number of Lagrangian parcels. At each time step, each particle is displaced according to the advective process (buoyancy, ambient current) with the velocity $\mathbf{U}$ and diffusive process (turbulent fluctuations). These particles are introduced at the end of the plume dynamics. Each particle displacement is as follows:

$$\frac{d\mathbf{X}}{dt} = \mathbf{U} + \mathbf{U}' \tag{36}$$

where $\mathbf{X}$ is the position vector of the particle (m) and $\mathbf{U}'$ the diffusive velocity (m/s). The diffusion is modelled using a random walk algorithm.

This fluctuating component of the current acting on particles is altered at each time step by a normal random deviation with amplitude specified by the root mean square of the fluctuating currents (Yapa, 1994):

$$\mathbf{U}' = V' R_n e_n^{i\theta} \tag{37}$$

with

$$V'_{x,y} = \sqrt{4 D_h / \delta t} \tag{38}$$

$$V'_z = \sqrt{2 D_v / \delta t} \tag{39}$$

In which δt the time step (s), D_h and D_v the horizontal and vertical diffusion coefficient (m^2/s) respectively. R_n is a normally distributed random number with a mean value of 0 and a standard deviation of 1. The directional angle θ' is assumed to be a uniformly distributed random angle ranging between 0 and π .

3.2.4 Boundary conditions

The plume dynamic stage (PDS) provides a source term to the advection diffusion stage (ADS). Parcels representing a large number of droplet/bubbles are created at the NBL and then follow the physical model. The boundaries conditions are:

- When reaching surface, HNS parcel are destroyed.
- When reaching seabed, HNS parcel are stucked.

The dissolution process leads to creation of dedicated parcel to track dissolved HNS in a liquid aqueous state. Their transport is similar to standard parcels, as they are governed by the same advection and diffusion processes.

3.2.5 Particle size distribution

Based on the initial droplet size distribution (DSD), particles are discriminated into a number of classes in both models. In the plume dynamic stage, the whole distribution is integrated into the control volume and is computed each time step. In the mass conservation equation, the dissolution term $\frac{dm_d}{dt}$ (kg.s^{-1}) is thus given by:

$$\frac{dm_d}{dt} = \sum_{i=1}^{k} \left(\frac{dn}{dt} \right)^i M \qquad (40)$$

Where k is the number of droplet size classes, $(dn/dt)^i$ is the HNS consumption rate by dissolution (mol.s^{-1}), and M the molecular weight of the HNS (kg.mol^{-1}).

In the advection-diffusion stage, each parcel at the NBL represents a number of droplet/bubble with a given class size among the final control volume DSD.

The related details of the dissolution rate computation are given in §3.2.7.

3.2.6 Particle slip velocity

In plumes, there is a slip velocity w_s between rising fluid particles and the surrounding liquid within the plume area. In a droplet plume, it is the velocity difference between rising droplets and the surrounding water. The most used law to calculate this slip velocity is based on the Stokes' law but it approximates only small bubbles considered as perfect spheres. Clift et al. (1978) have shown that the shape of fluid particles could be approximated as a sphere for the small size range (smaller than 1 mm), an ellipsoid in the intermediate size range (1 mm to 15 mm), and a spherical-cap in the larger size range. They also demonstrated that shape has an important impact on the particle terminal velocity.

For spherical bubbles the terminal velocity is influenced by the viscosity of the ambient fluid; for ellipsoidal bubbles the interfacial tension is the key factor, while neither the viscosity of the ambient fluid or interfacial tension influence spherical-cap bubbles.

Clift et al. (1978) offer several correlations for the different regimes of bubble shapes.

- The regime of spherical shape is given by:

$$w_s = \frac{\mu R_e}{\rho d} \quad (41)$$

where R_e is the Reynolds number, μ the dynamic viscosity of ambient water (Pa.s), ρ the density of ambient fluid (kg/m^3) and d the spherical particle diameter (m).

- The regime of ellipsoidal shape is given by:

$$w_s = \frac{\mu}{\rho d_e} M^{-0.149} (J - 0.857) \quad (42)$$

where d_e is the equivalent diameter (m), and:

$$J = 0.94H^{0.757} \qquad \text{for } 2 < H \leq 59.3$$

$$J = 3.42H^{0.441} \qquad \text{for } H > 59.3$$

H is defined as $H = \frac{4}{3} E_o M^{-0.149} \left(\frac{\mu_l}{\mu_w}\right)^{-0.14}$ with μ_w the dynamic viscosity of water (Pa s^{-1}).

E_o the Eötvös number defined as follows : $E_o = \frac{g(\rho_w - \rho_l)d^2}{\sigma}$ with σ the interfacial tension between the fluid and the water (N m^{-1}),

M the Morton number defined by $M = \frac{g(\rho_w - \rho_l)\mu^4}{\rho_w^2 \sigma^3}$

The criteria in this regime are M<10^{-3} and Eo<40.

- The regime of spherical-cap is given by:

$$w_s = 0.711 \sqrt{\frac{g(\rho_w - \rho_l)d^2}{\rho_w}} \quad (43)$$

The Clift's law has been well validated with five chemical products (n-butanol, ethyl acetate, methyl metacrylate, methyl isobutyl ketone, methyl ter butyl ether). Details on comparisons and figures are in the technical report for HNS-MS "*Characterization of the HNS behaviour in the water column*" (Aprin 2016).

3.2.7 Dissolution model

In the context of the project HNS-MS, a short review of some models dealing with HNS chemicals is done. Literature articles generally consider only one aspect: Either surface slick is considered or single liquid droplet in the water column (especially in a liquid/liquid extraction topic). In our research, no scientific articles dealing with HNS dissolution covering both compartments where found. It can be explained by:

- The recent interest in modelling chemical fate at sea, while oil focus efforts for decades,
- The weak probability of a scenario of a subsea leakage of a dissolver HNS, and the recent realization about pollutions environmental impacts.

In academic or commercial projects dealing with chemical at sea and their fate, dissolution of surface spillet and re-immersed chemical droplets are generally considered in an analogous way, detailed later.

The CLARAII (2010) project was dedicated to the evaluation of impacts of accidental release in the Mediterranean sea. Dissolution computation was included, for both surface and water column compartment, and largely inspired by CHEMMAP model.

CHEMMAP (French and Isaji, 2004) is a commercial product developed by ASA, which predicts the trajectory, fate, impacts and biological effects of discharged chemical substances. It is currently used by CEDRE in operational or training contexts. In CHEMMAP, dissolution is applied on pure substances and on chemical from a hydrophobic solvent slick or suspended droplet. The model algorithm follows the work of Mackay and Leinonen (1977) and Hines and Maddox (1985): the slick (spillet) is treated as a flat circular plate, with a mass flux related to solubility and temperature. It assumes a well-mixed layer with most of the resistance to mass transfer lying in the hypothetically stagnant region close to the slick. For subsurface droplets, dissolution is also treated as a mass flux but across the spherical surface area of a droplet, in a calculation similar to the slick algorithm.

The number of dissolved moles mass $n_{i,d}$ (moles) of i^{th} component (chemical) is given by:

$$\frac{dn_{i,d}}{dt} = K(x_i C_i^s - C_i^w)A \qquad (44)$$

where the surface area of slick or particle A is in cm^2, the dissolution mass transfer coefficient K is in cm s^{-1}, the solvent phase mole fraction of i^{th} component x_i (1.0 for pure chemicals), the pure component solubility of i^{th} component C_i^s (mol cm^{-3}) and the actual concentration of i^{th} component in the water phase C_i^w (mol cm^{-3}).

3.2.7.1 Surface slick

The mass transfer coefficient K_s (m s^{-1}) for a surface slick is given by:

$$K_s = \frac{ShD_C}{L} \quad (45)$$

Where Sh is the average Sherwood number, L the diameter of a surface slick (m) and D_C the diffusion coefficient taken at 25°c (m^2 s^{-1}). It is estimated using the Hayduk and Laudie (1974) method described in Lyman et al. (1982), calculated in cm^2 s^{-1} :

$$D_C = \frac{13.26 \times 10^{-5}}{\mu^{1.14} v_l^{0.589}} \quad (46)$$

where μ the dynamic viscosity of water is in centipoises and the Le Bas molar volume v_l in cm^3 mol^{-1}. In CHEMMAP, the "Le Bas" molar volumes of representative organic or inorganic chemicals were regressed against molecular weight to derive the following models:

$$\begin{cases} v_l = 4.9807 \times M_w^{0.6963}, & \text{for organic chemicals} \\ v_l = 2.8047 \times M_w^{0.651}, & \text{for inorganic chemicals} \end{cases} \quad (47)$$

with v_l in (m^3 mol^{-1}) here, and M_w the molecular weight (g mol^{-1}).

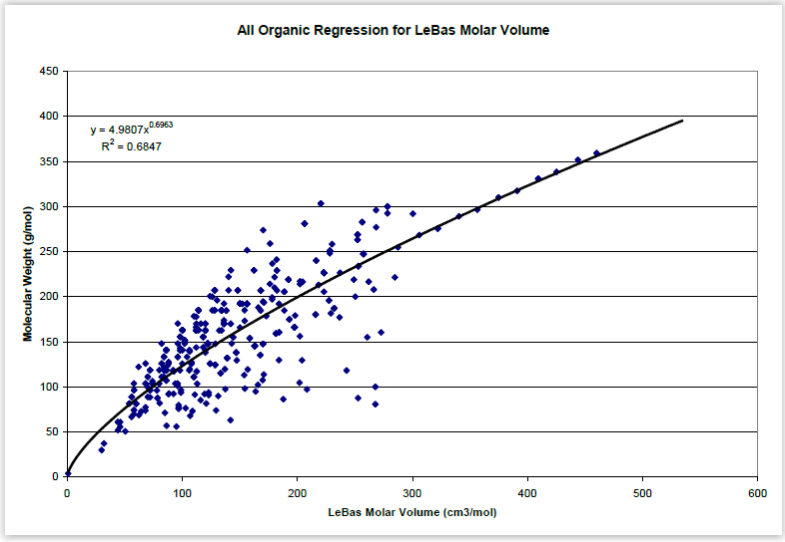

Figure 25 : Organic Regression for Le Bas Molar Volume (CHEMMAP Technical User's Manual 2014 Version 6.10)

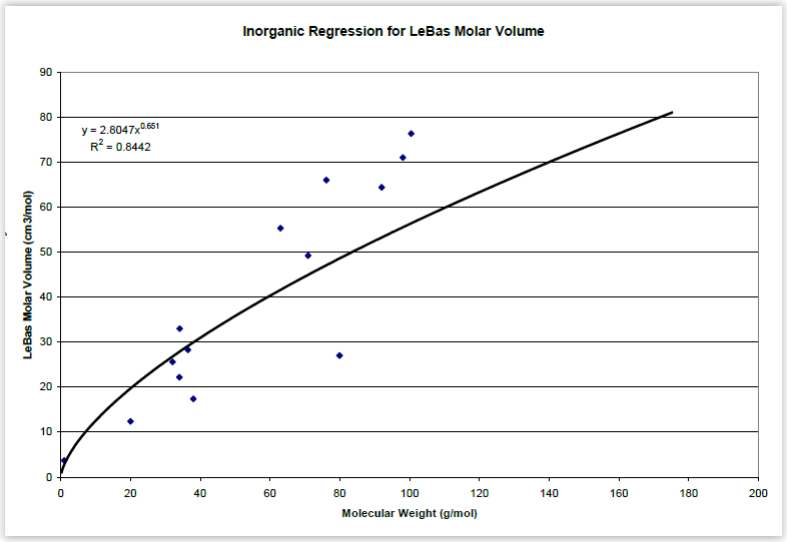

Figure 26 : Inorganic Regression for Le Bas Molar Volume (CHEMMAP Technical User's Manual 2014 Version 6.10)

The Le Bas molar volumes (organic and inorganic chemicals) come from MacKay et al. handbooks (1992). In its recent version, the molar volume at the normal boiling point is estimated by the Le Bas method (Reid et al. 1987), consisting in a summation of atomic volumes, with adjustment for the volume decrease arising from ring formation (Figure 27).

	Increment, cm³/mol	
	Schroeder	Le Bas
Carbon	7.0	14.8
Hydrogen	7.0	3.7
Oxygen	7.0	7.4
In methyl esters and ethers		9.1
In ethyl esters and ethers		9.9
In higher esters and ethers		11.0
In acids		12.0
Joined to S, P, and N		8.3
Nitrogen	7.0	
Doubly bonded		15.6
In primary amines		10.5
In secondary amines		12.0
Bromine	31.5	27.0
Chlorine	24.5	24.6
Flourine	10.5	8.7
Iodine	38.5	37.0
Sulfur	21.0	25.6
Ring, three-membered	−7.0	−6.0
Four-membered	−7.0	−8.5
Five-membered	−7.0	−11.5
Six-membered	−7.0	−15.0
Naphthalene	−7.0	−30.0
Anthracene	−7.0	−47.5
Double bond	7.0	
Triple bond	14.0	

Figure 27 : Le Bas molar volume

The evaluation of the mass transfer coefficient K_{d_s} depends on the average Sherwood number given by :

$$Sh = 0.578 Sc^{1/3} Re_L^{1/2} \quad (48)$$

where Sc is the Schmidt number, and Re_L is the Reynolds number. These numbers are respectively:

$$Sc = \frac{\nu_w}{D_C} \quad (49)$$

where $\nu_w = 10^{-6}\,\mu_w/\rho_w$ the kinematic viscosity of water (m s), and the Reynolds number :

$$Re_L = \frac{U_w L}{\nu_w} \quad (50)$$

with U_w the wind speed, in m s^{-1}.

For subsurface droplets, the mass transfer coefficient K_d (m s^{-1}) is given by:

$$K_d = \frac{ShD_C}{d} \quad (51)$$

where Sh is the average Sherwood number, d the diameter of the droplet (m) and D_C the diffusion coefficient taken at 25°c (m^2 s^{-1}). For this case, the Sherwood number is:

$$Sh = 2 + 0.347Sc^{0.31}Re_d^{0.62} \quad (52)$$

where Re_d is the Reynolds number based on droplet diameter :

$$Re_d = \frac{W_d d}{\nu_w} \quad (53)$$

with W_d the resultant velocity action on the droplet in m s^{-1}.

The ARCOPOL+ project (Rodrigo Fernandes, 2012) proposed the same approach for modelling dissolution. It is estimated for spillets in the surface, based on the hypothesis of a flat plate (the slick), and for the water column, dispersed droplets are assumed to be spherical. Dissolution is treated as a mass flux across the surface area of the flat plate/sphere, according to MacKay and Leinonen (1977) once again.

The dissolution flux equation is similar, with an additional term taking account for the type of concerned hydrocarbon (alkanes, aromatics, etc.):

$$\frac{dn_{i,d}}{dt} = K(e_i x_i C_i^s - C_i^w) \quad (54)$$

Where the dissolution mass transfer coefficient K is in cm s^{-1}, e_i the solubility enhancement factor having values given in (MacKay and Leinonen, 1977), x_i the pollutant phase mole fraction, C_i^s the pure component solubility (mol cm^{-3}) and C_i^w the bulk water phase concentration of i (mol cm^{-3}).

Hydrocarbon	e_i
alkanes	1.4
cycloalkanes	1.4
aromatics	2.2
olefins	1.8

Figure 28 : Solubility enhancement factor

In the ARCOPOL+'s dissolution model, the mass transfer coefficient is assumed to be constant to 2.36×10^{-4} cm s^{-1}.

A more recent work (Fernandez PhD thesis, 2013) has been done on modeling spreading and vaporization phenomena of multicomponent pools for the "Phast" software. The model accounts for spills on land and water surfaces, and the dissolution is introduced and deals with water soluble chemicals present in the mixture. Following equations presented by Dodge et al. (1983), the model treats dissolution for open bodies of water as lakes and coastal waters, considering effects of waves and surface roughness, dependent on the wind velocity. The flux of dissolved chemical is estimated as a function of the solubility of the chemical and the water surface properties. Like before the mass transfer is given by:

$$k_w = \frac{m''_{sol}}{\rho_w (w_s - w_\infty)} \quad (55)$$

where k_w the overall mass transfer coefficient across the pool water interface (m s^{-1}), m''_{sol} the mass flux of the chemical dissolved in water (kg m^{-2} s^{-1}), ρ_w the ambient water density (kg m^{-3}), w_s and w_∞ respectively the mass fraction of the chemical in water at the pool-water interface and in the water bulk (=0). A correction factor for high mass transfer rates is used based on Witlox 2008:

$$m''_{sol} = k_w \rho_w \ln\left(\frac{1}{1 - w_s}\right) \quad (56)$$

For open and coastal waters (Dodge et al. 1983), the mass transfer coefficient is given by:

$$k_w = 10 \frac{u_w^*}{\frac{\sigma \ln(\delta_+)}{\varphi} + \beta_w + 2.35} \quad (57)$$

$$\delta_+ = \frac{10 u_w^* \rho_w}{\mu_w} \quad (58)$$

$$\beta_w = \begin{cases} 12.5Sc^{0.667} + \dfrac{\sigma ln(Sc_w)}{\varphi} - 5.3, & u_{(z=10m)} < 5m/s \\ 0.55h_w^{0.5}\left(Sc_w{}^{0.667} - 0.2\right) - \dfrac{\sigma ln(Sc_w)}{\varphi} + 11.2\sigma, & u_{(z=10m)} \geq 5m/s \end{cases} \quad (59)$$

$$h_w = 0.01384 \frac{u_{(z=10m)} u_w^* \rho_w}{\mu_w} \quad (60)$$

$$u_w^* = u_{(z=10m)} \left(\frac{\rho_a}{\rho_w}\right)^{1/2} \left(\frac{1}{2} C_f\right)^{1/2} \quad (61)$$

$$\frac{1}{2} C_f = \begin{cases} 1.98 \times 10^{-3} & u_{(z=10m)} < 0.1m/s \\ 1.25 \times 10^{-3}\left[u_{(z=10m)}\right]^{-0.2} & 0.1 < u_{(z=10m)} < 3.06m/s \\ \left[0.8 + 0.065u_{(z=10m)}\right] \times 10^{-3} & 3.06 < u_{(z=10m)} < 22.3m/s \\ 2.25 \times 10^{-3} & 22.3m/s < u_{(z=10m)} \end{cases} \quad (62)$$

where δ_+ the height of the boundary layer formed between the pool and the water surface (m), β_w an empirical function dependent on the surface roughness, h_w the wave height (m), C_f the friction coefficient at the water-pool interface, $u_{(z=10m)}$ the wind speed measured at 10m above the pool (m.s^{-1}), φ the Von Karman constant (=0.41), σ the turbulent Schmidt number (=0.8).

3.2.7.2 Subsurface droplet

Wegener et al. (2014) worked on the mass transfer coefficient evaluation for subsurface droplet. Because of the complexity of swarm systems for subsurface liquid-liquid extraction, they adopted the position of reducing the problem to droplets as they are the smallest mass transfer unit. Based on a literature survey, they pointed the fact that the description of droplets in liquid is more complicated than bubbles in liquids, or rigid particles in gas, because in both cases the extreme viscosity ratio (0 or ∞) simplifies modeling. Depending on the resistance mechanism between the dispersed and the continuous phase, they divided it in three cases for circulating droplet with mobile interface:

- The external problem when resistance is mainly in ambient phase

$$\left(K^* \sqrt{D_{A,d}/D_{A,c}} \gg 1\right) \quad (63)$$

- The internal problem when resistance is mainly in dispersed phase

$$\left(K^* \sqrt{D_{A,d}/D_{A,c}} \ll 1\right) \quad (64)$$

- The conjugated problem, when resistance is in both phases

$$\left(K^* \sqrt{D_{A,d}/D_{A,c}} \approx 1\right) \quad (65)$$

For the external problem, Clift et al (1978) correlations are used to estimate the mass transfer coefficient, depending on particle size like bubble.

Focused on the conjugate problem, authors pointed out some aspects in the mass transfer estimation, often neglected in literature models: the droplet formation stage, the Marangoni convection and the influence of contaminations or surfactants. The transferred mass during droplet formation M_s, is given by:

$$M_s = \frac{6}{7} d_{Pf}^2 \Delta C_s (\alpha D_s \pi t_c)^{1/2} \quad (66)$$

where d_{Pf} is the droplet formed diameter (m), α is a diffusivity factor, D_C is the diffusion coefficient ($m^2.s^{-1}$), t_c is the sum of the droplet formation time (s). α is linearly regressed as a function of the initial solute concentration C_{s0} (g L^{-1}), and for the "dispersed to continuous" direction, the equation is :

$$\alpha = 3.08 + 0.1765 C_{s0} \quad (67)$$

In the free rising/falling of the droplet, variation of the interfacial tension of the droplet and Marangoni convection effects have to be considered. Kumar and Hartland (1999) proposed a

correlation based on 200 data points published by several groups of investigators in different single droplet systems, including, circulating and oscillating droplets to estimate the Sherwood number for the dispersed phase:

$$Sh_d = 17.7 + \frac{3.19 \times 10^{-3}\left(ReSc_d{}^{1/3}\right)^{1+\alpha}}{1 + 1.43 \times 10^{-2}\left(ReSc_d{}^{1/3}\right)^{\alpha}} \frac{\rho^{*2/3}}{1+\mu^{*2/3}} \quad (68)$$

where $\alpha = 0.7$, the Schmidt number $Sc_d = \mu_d/(\rho_d D_{sd})$, the Reynolds number Re, the density ratio ρ^*, the viscosity ratio μ^*. The Reynolds number Re has to reflect the corrected velocity of the droplet, affected by Marangoni convection.

3.2.7.3 Subsurface bubble

Wüest et al. (1992) developed a gas plume model for the restoration of deep stratified lakes, using O_2 or N_2 gases. The plume model includes gas dissolution. They evaluate the gas flux Q_b through bubble surfaces (mol m^{-2} s^{-1}) from the following:

$$Q_b = \beta_i(C_{si} - C_i) \quad (69)$$

Where β_i is the mass transfer coefficient (m s^{-1}) for the gas species i (O_2 or N_2), C_i is the in situ dissolved gas concentration (mol m^{-3}), and C_{si} is the saturation concentration (mol m^{-3}) determined by Henry's law:

$$C_{si} = K_i p_i \quad (70)$$

p_i is the in situ partial pressure of the gas phase of species i and $K_i$is the solubility constant (mol m^{-3}). The solubility of molecular nitrogen and oxygen are functions of temperature using a second order polynomial fit to experimental data from Marshall (1976).

Zheng and Yapa (2002) proposed an equivalent formula to compute the gas dissolution in the context of an oil/gas spill, including deep water release. Based on a lagrangian approach, the jet/plume is tracked through consecutive volumes of control, composed of a mixture of entrained water, oil, gas bubbles and subjected to chemical reactions such as gas dissolution. The dissolution rate of a bubble $\frac{dn}{dt}$ (mol.s^{-1}) is calculated from a mass transfer coefficient and solubility of gas in water:

$$\frac{dn}{dt} = KA(C_s - C_0) \quad (71)$$

n is the number of moles of gas in a bubble (mol), K is the mass transfer coefficient (m s^{-1}), A the surface area of gas bubble (m^2), C_0 the concentration of the dissolved gas in ambient water (mol.m^{-3}) and C_s the saturated value of C_0 (mol.m^{-3}). Gas solubility is valid for low and high

pressure and the mass transfer coefficient can be applied to different gases and different shapes of bubbles.

The saturated value or solubility is given by:

$$C_s \approx x^l \frac{\rho_l}{M_l} \quad (72)$$

with x^l the mole fraction of dissolved gas in water at equilibrium condition, ρ_l the water density (kg.m^{-3}) and M_l the molecular weight of water (kg.mol^{-1}). The solubility of gas in water is calculated by the Henry's law:

$$P = Hx^l \quad (73)$$

where P is the gas pressure (Pa), H is the Henry's law constant (Pa) which is dependent on the water temperature. This Henry's law is limited to low pressure of ideal gas. Then, for deep water, a modified Henry's law based on fugacity can be used:

$$f_g = Hx^l \exp\left(\frac{P\nu_l}{RT}\right) \quad (74)$$

with $R = 8.31$ the universal gas constant, T the water temperature (K), ν_l the molar volume of gas (m^3.mol^{-1}). The solubility of gas in water is strongly dependent on the ambient pressure, temperature and salinity. In deep water with high pressure, the ideal gas law breaks down. We have to consider the behaviour of a real gas described as follows:

$$PV = ZnRT \quad (75)$$

with Z the compressibility factor. The fugacity and the compressibility factor can be calculated with the Peng-Robinson equation-of-state.

The effect of salinity on solubility is discussed in Zheng et al. (2002). Weiss (1974) and Yamamoto et al.'s (1976) showed that the Henry's law constant in seawater is 15% and 20% lower than in distilled water for CO_2 and CH_4 respectively.

The mass transfer coefficient of gas bubbles in liquids is dependent on the size and shape of bubbles as well as gas diffusivity in liquids. Small size bubbles can be approximated as spheres, intermediate size bubbles as ellipsoids, and large size bubbles as spherical-caps. Zheng and Yapa (2002) and McGinnis et al. (2006) combined the equations originally developed by Johnson et al. (1969) and Clift et al. (1978):

$$\begin{cases} K = 1.13\left(\frac{w_b}{0.45 + 0.2d_e}\right)^{1/2} D^n & , \quad d_e \text{ from 0 to 0.5 cm} \\ K = 6.5D^n & , \quad d_e \text{ from 0.5 to 1.3 cm} \\ K = 6.94 d_e^{-1/4} D^n & , \quad d_e > 1.3 \text{ cm} \end{cases} \quad (76)$$

The diffusion coefficient D is in cm^2 s^{-1}, the slip (or terminal) velocity w_b is in cm.s^{-1} and is the equivalent diameter in cm. The diffusion exponent, n, varies from $1/2$ to $2/3$ for clean bubbles and dirty bubbles, respectively. The diffusion coefficient computation is based on Hayduk and Laudie (1974), and reported in §3.2.7.1.

3.2.7.4 Comparisons with CEDRE-EMA experiments

In the scope of the HNS-MS project, CEDRE and EMA performed experiments in the water column (task D.3). All related details can be found in the technical report "*Characterization of the HNS behaviour in the water column*" (Aprin, 2016). For five different chemicals, evolution of the droplet diameter and variation of the volume have been observed based on size distribution recorded at the bottom and at the top of the column.

3.2.7.4.1 Simulation configurations

The dissolution model is tested through ChemSPELL (Chemical Subsea Plume ModEL for Leakage) the near-field part of HNS-MS Decision Support System tool. The experimental configuration is not directly reproducible because of the very low flow rate used (0.25 ml.min^{-1} to 2.15 ml.min^{-1}) and the nozzle diameter (5 mm), which can't be supported by ChemSPELL. Moreover experiments tend to have unique droplets at the orifice, generally with the same size. Indeed droplet size distribution is limited to one or two size classes in mm, for the five chemicals.

The following adaptations have been done on ChemSPELL initialization:

- The nozzle diameter is taken to 1cm, and the flow rate is evaluated with respect to the release velocities of experiments. The reason is that the rising velocity of a droplet has an important impact on dissolution.
- The release point is taken to the bottom observation height, and the drop size distribution is forced to the bottom mean diameter observed.

Temperature, salinity, and distance between the two observation points have been respected. Substances physical and chemical properties such as density, hydrosolubility (fresh water), dynamic viscosity and interfacial tension presented in the report have also been used here. Those values were taken at 20°c or 25°c, for all the substances, while water temperature during the experiments was about 18°c. That approximation is acceptable as the change in properties is negligible.

The purpose of the comparisons is to find the best dissolution model for subsea droplet, between those presented in §3.2.7.2. As a consequence, four configurations have been tested (Table 6). Cases include a reduction factor on dissolution due to the salinity effect: Hydrosolubility provided are values for fresh water, and it appears to be relevant to introduce a coefficient for the comparisons to feel the sensitivity of that environmental parameters on dissolution models.

	ChemSPELL "A"	ChemSPELL "B"	ChemSPELL "C"	ChemSPELL "D"
Dissolution model	eq. (68)	eq. (68)	eq. (52)	eq. (52)
Salinity effect limitation factor	No factor	50%	No factor	50%

Table 6 : ChemSPELL configurations for dissolution comparisons with CEDRE-EMA experiments

3.2.7.4.2 Results comparisons and discussion

Results of the ChemSPELL simulations are summarized in Table 7. Droplet mean diameters at bottom and top of the column from experiments are precised. Droplet diameters for the five chemicals and for the four configurations are compared to the experimental value with the relative errors on diameter. Variations of the droplet volume are also presented.

As explained above, configurations "A/B" and "C/D" corresponds respectively to the two dissolution models implemented in ChemSPELL, one from Mackay and Leinonen (1977), the other from Kumar and Hartland (1999). Results are much better for configurations "C" and "D" with a mean relative error on the five chemical of 3.6%, against 33% for configurations "A" and "B".

Another interesting result is the comparisons with an applied reduction coefficient: the hydrosolubility for fresh water makes the model overestimates the dissolution. Indeed the salt in water has an inhibition effect on HNS dissolution (Xie et al 1997). Configurations "B" and "D" show that they both improve the behaviour as the relative error on the droplet diameter decrease, with values of 14.3% and 2.9 % respectively. Two extended tests based on configuration "D", which are not reported here, have been conducted with a limitation coefficient of 80% and 20%. Results are less good, with mean relative errors of 3.3% and 4.2% respectively.

Comparisons with CEDRE-EMA experiments have shown some relevant results:

- The dissolution model for subsea droplets from Mackay and Leinonen (1977) provides better results, and is selected for ChemSPELL and the dissolution module. Reasons on

the important deviation between the two models are not easy to identify, and would require other experimental data to reinforce that observation.

- The effect of the salinity as an inhibitor of chemical dissolution has been well observed. In order to make up the use of hydrosolubility for fresh water, a reduction coefficient has been introduced in ChemSPELL simulations for the tests, and it appears that the 50% limitation coefficient case provides the minimum relative error, which is in very good agreement with observations of Xie et al (1997) that considers a solubilisation in salt water about two times slower than in fresh water.

Concerning the surface slick dissolution model, Mackay and Leinonen model is privileged, just like for subsea droplet, even if no comparisons have been performed. For both context - surface/subsea - further investigations and experiments on chemical dissolution would be interesting in order to confirm and refine dissolution models.

Chemical	n-butanol	Ethyl acetate	Methyl metacrylate	Methyl Isobutyl Ketone (MIK)	Methyl Ter Butyl Ether (MTBE)
Exp. drop diameter (bottom)	1.50 mm	3.75 mm	5.39 mm	3.74 mm	3.34 mm
Exp. drop diameter (top)	1.25 mm	3.56 mm	5.40 mm	3.63 mm	3.22 mm
ChemSPELL "A" drop diameter (top)	1.26 mm	1.94 mm	4.99 mm	3.35 mm	1.95 mm
ChemSPELL "B" drop diameter (top)	1.38 mm	2.73 mm	5.19 mm	3.54 mm	2.57 mm
ChemSPELL "C" drop diameter (top)	1.25 mm	3.26 mm	5.31 mm	3.64 mm	3.01 mm
ChemSPELL "D" drop diameter (top)	1.37 mm	3.51 mm	5.35 mm	3.69 mm	3.18 mm
ChemSPELL "A" drop diameter relative error	0.6 %	83.6 %	8.2 %	8.4 %	65.2 %
ChemSPELL "B" drop diameter relative error	9.4 %	30.5 %	4.0 %	2.5 %	25.2 %
ChemSPELL "C" drop diameter relative error	0.2 %	9.1 %	1.7 %	0.2 %	6.9 %
ChemSPELL "D" drop diameter relative error	9.0 %	1.5 %	0.9 %	1.6 %	1.4 %
Exp. mean drop volume variation	46 %	16 %	0 %	6 %	12 %
ChemSPELL. "A" mean drop volume variation	41 %	86.2 %	20.5 %	28.1 %	80.1 %
ChemSPELL. "B" mean drop volume variation	22.3 %	61.5 %	10.6 %	15.1 %	54.4 %
ChemSPELL. "C" mean drop volume variation	41.8 %	34.1 %	4.5 %	8.0 %	26.7 %
ChemSPELL. "D" mean drop volume variation	23.2 %	18.2 %	2.2 %	4.0 %	14.0 %

Table 7 : Comparisons between ChemSPELL and CEDRE-EMA experiments for dissolution of five chemicals in a water column

ChemDRIFT
HNS-MS far field model

PAGE INTENTIONALLY LEFT BLANK

4 ChemDRIFT, HNS-MS far-field model

4.1 Introduction

The objective of the ChemDRIFT model is to simulate the drift, behaviour and fate of liquid or granular solid (and powder) HNS spilt in the marine environment for the first few days (1-5) after the spillage. Because the timescale and processes involved in this context are quite similar to those implemented in RBINS oil spill drift and fate model OSERIT (Dulière et al., 2013), ChemDRIFT implementation is an in-depth evolution of the OSERIT model.

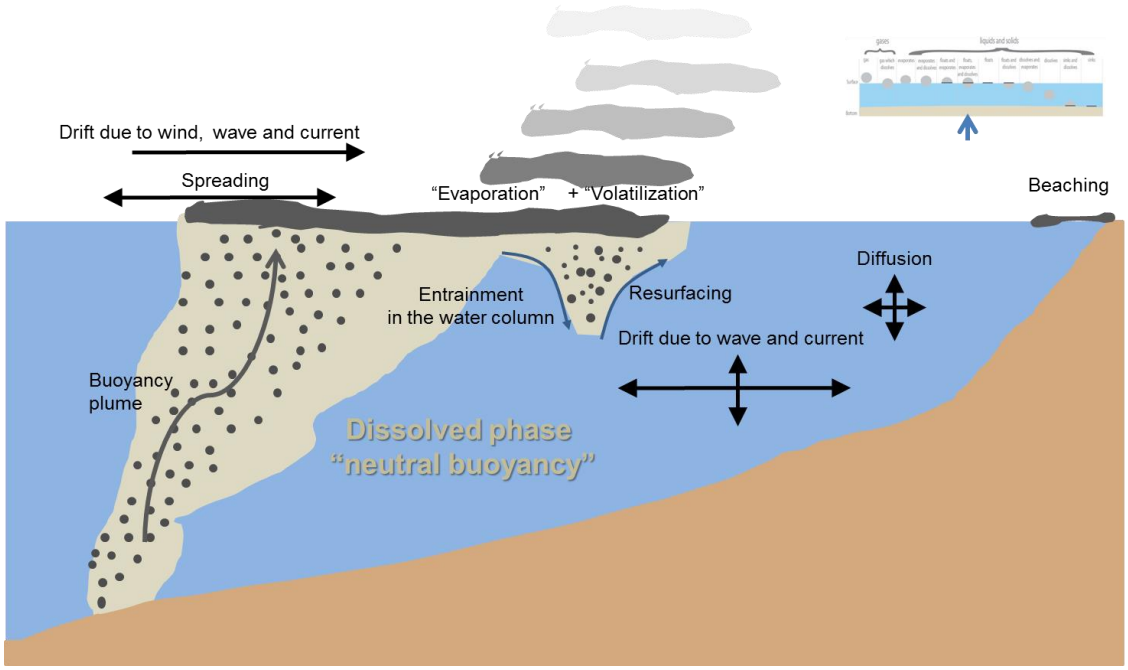

Figure 29: Schematic representation of the processes included in ChemDRIFT

ChemDRIFT model follows a kinetic approach based on empirical data and parameterizations that simulates the 3D drift, behaviour and fate of HNS at the sea surface, in the water column and at the seabed (Figure 29). It is based on the Lagrangian particle tracking method that represents spilt HNS by a cloud of tens or hundreds of thousands of particles to which is associated a fraction of the total HNS mass. The Lagrangian module computes the displacement of each particle independently under the combined action of the wind, water current and wave. The model also includes the buoyancy effect, turbulent diffusive transport, vertical natural dispersion of surface oil into the water column, horizontal surface spreading, dissolution, evaporation, sedimentation and beaching. Biodegradation is not included in the model since it usually is a slower process with relatively little impact on the HNS behaviour during the very first days. At the difference of OSERIT, ChemDRIFT does not include emulsification because no HNS listed in the HNS-MS database forms stable emulsion when spilt at sea. Finally, because ChemDRIFT currently only simulates the drift, behaviour and fate of pure HNS, no weathering

processes are included. The model can be run forwards in time to provide forecast of the HNS spill drift, behaviour and fate or backwards in time to provide a backtracking of the HNS spill. However, because many processes are not reversible in time, backtracking simulations are subject to strong restrictions. For a maximum flexibility, each process implemented in the model can be activated (or deactivated) by designated model switches.

4.2 ChemDRIFT philosophy

4.2.1 Understanding the concept behind ChemDRIFT's Lagrangian particles

The Lagrangian particle is the basic conceptual object of the ChemDRIFT model. Because a fraction of the total pollutant is associated to each particle, ChemDRIFT end-users should interpret the time evolution of a ChemDRIFT Lagrangian particle in a way that is consistent with the expected time evolution of the associated pollutant fraction. Indeed, in function of the total HNS volume released in the marine environment and the total number of Lagrangian particles considered in the simulation[6], the amount of pollutant associated to each particle can represent several (tens of) litres of pure HNS. This volume of pollutant can take one of the following 9 physical states:

1. **Evaporated fraction in the air** - this fraction is considered to be out of the ChemDRIFT model area.
2. **Liquid fraction at the sea surface** – it is assumed that this fraction contributes to the formation of a continuous slick at the sea surface. The thickness of the slick depends on the total volume of the HNS liquid at the sea surface and the surface of the slick. This fraction can further change as a function of evaporation, dissolution and natural entrainment in the water column.
3. **Granular solid fraction at the sea surface –** it is assumed that this fraction is distributed into n_l small balls with a median diameter d. As a function of their diameter, these balls can be view as material grains, powder lumps or pellets. By default, the initial ball diameter is of 10cm, but this value can be adjusted by the model operator. The number n_l of balls is computed in order to conserve the total mass associated to the particle. The size of the balls can then evolved in time as a function of dissolution. No sublimation is considered.
4. **Liquid fraction in the water column** – it is assumed that this fraction is distributed into n_d droplets of median diameter d. This maximal droplet diameter is a function of the liquid density and interfacial tension. The number n_d of droplets is computed in order to

[6] As a rule of thumb, the maximal volume of HNS associated to a single particle should correspond to a limit of detection or to a limit of toxicity.

conserve the total pollutant mass associated to the particle. The droplet size can evolve in time as a function of dissolution.

5. **Granular solid fraction in the water column –** it is assumed that this HNS mass fraction is distributed in n_l small balls of median diameter d. These balls can be view as material grains, powder lumps or pellets of a given size. The number n_l of balls is computed in order to conserve the total mass associated to the particle. The median balls diameter can evolve in time as a function of lumps dissolution.
6. **Dissolved fraction in the water column** – it is assumed that this HNS mass fraction is indistinguishable with the surrounding sea water. It therefore has no buoyancy effect. If ChemDRIFT neglects the interaction with suspended particulate matter, the dissolved fraction in the direct vicinity of the sea surface can be volatilized.
7. **Liquid fraction at the sea bed** – it is assumed that a liquid particle sunk at the seabed, contributes to the formation of a slick covering the seabed. ChemDRIFT does not allow the resuspension of this slick. The dissolution process can continue.
8. **Solid fraction at the seabed** – it is assumed that the solid balls sunk at the seabed can neither be resuspended in the water column nor roll on the seabed: sunk balls cannot drift anymore. The dissolution process can continue.
9. **Beached fraction** – In ChemDRIFT, beaching occurs when a liquid or solid particles floating at the sea surface reaches the coastline.

4.2.2 Statistical interpretation of the spill macroscopic features

If the Lagrangian particles method assumes that each particle evolves in space and time independently of the other particles, macroscopic features of the spill such as the mass balance diagram can only be computed considering the whole particles cloud properties and therefore must be understood in a statistical way.

Similarly, spatially-dependent macroscopic spill features such as HNS concentration and HNS slick thickness can be computed from particles subsets. The subset size must be large enough to be statistically relevant and small enough so that the macroscopic features can be assumed homogeneous on the area/volume covered by the subset.

After having considered several sub-setting/clustering methods such as nearest neighbours, Voronoï tessellation and quadtrees/octrees, we find out that the most efficient clustering strategy for our purpose is a flavour of the quadtree approach for which all leaves (our sub-setting bins) are defined at the same zoom level; the zoom level 0 corresponding to the metocean forcing grid. The south-west corner of the subsetting bin i,j for the zoom level k is therefore located at the following longitude and latitude:

$$\begin{cases} \lambda_{i,j}^{k} = \lambda_0 + i\left(\frac{1}{2}\right)^k d\lambda_0 \\ \varphi_{i,j}^{k} = \varphi_0 + j\left(\frac{1}{2}\right)^k d\varphi_0 \end{cases}$$

The horizontal resolution of the different zoom level is given in Table 8. The vertical resolution of the sub-setting bins are computed following the same methodology for unequally spaced sigma coordinates levels, with the restriction that the a sub-setting bin cannot be thinner than one meter.

Table 8: Horizontal resolution of the sub-setting bins in function of the zoom level

Zoom level k	0	1	2	3	4	5	6	7
Resolution	~7000m	~3500m	~1750m	~0.875m	~437m	~218m	~110m	~55m

The adequate zoom level is defined in such a way that there are, in average, between 10 and 100 Lagrangian particles per active sub-setting bin. For a Lagrangian particles cloud made of 10000 particles, this means there is between 100 and 1000 active clusters of particles.

The Lagrangian particles moving independently from each other, the particles sub-setting must be done at each model timestep ($\Delta t_{drift} = 10$ minutes). To speed up the clustering, the most adequate zoom level is derived from the zoom level of the previous timestep.

Because of the homogeneity hypothesis, the mass and volume fractions of HNS associated to the particles belonging to the same cluster, can be added :

Because of the homogeneity hypothesis, evaporation (that depends on the slick area and the HNS volume) and dissolution (that depends on the dissolved concentration, the slick area or the droplets diameter) can be computed at the cluster scale. To do the different volume and mass fraction of the particles belonging to the same cluster are summed up. Once the evaporation and dissolution is computed ($\Delta t_{evaporation} = \Delta t_{dissolution} = 1$ minute), the total HNS mass and volume of the cluster can be redistributed among the different particles of the cluster in such a way that the most particles have only one physical phase. The latter mass redistribution trick allows to keep the number of active particles rather constant for the whole simulation and also simplifies the computation of the particle displacement at the next time step.

4.3 Mathematical model

4.3.1 Processes driving HNS spill drift and behaviour at the sea surface

4.3.1.1 Advection [all floaters]

The process of advection at the surface of the sea is dominated by winds, water currents and waves. Advection velocities are computed as follows:

$$\left\langle \vec{u} \right\rangle = D\,\vec{u}_w + \alpha_c \vec{u}_c + \vec{u}_{wave}$$

Where $\vec{u}_w$ is the wind velocity at 10 m above the surface; α_c is the current drift factor; $\vec{u}_c$ is the horizontal water current at the sea surface; $\vec{u}_{wave}$ stands for the advection component due to waves (or Stoke's drift). Because of their profile asymmetry and to surface gravity waves, drifting objects do not always drift directly downwind. There is often a significant component of the drift that is perpendicular to the downwind direction. D is the transformation matrix which allows introducing a deviation angle:

$$D = \begin{Bmatrix} \alpha_{dw} & \alpha_{cw} \\ -\alpha_{cw} & \alpha_{dw} \end{Bmatrix}$$

α_{dw} and α_{cw} are the wind drift factors in the downwind and crosswind directions, respectively.

Due to the lack of information reported in the literature, the values of the downwind and crosswind factors of HNS spills are parameterized following the classical parameterisation used for oil spills:

$$\alpha_{dw} = \alpha \cos(\vartheta)$$
$$\alpha_{cw} = \alpha \sin(\vartheta)$$

Where α is taken as 3.15%. ϑ is equal to $40° - 8\sqrt{|\vec{u}_w|}$ when $0 \le |\vec{u}_w| \le 25\ m/s$ and $\vartheta = 0$ when $|\vec{u}_w| > 25\ m/s$.

Liquid slick and drifting objects are moving along with waves, following orbital motions that are not closed. This results in a net particles transport in the direction of wave propagation known as the Stoke's drift. The drift velocity associated with waves is computed as in Daniel et al. (2003):

$$u_{wave} = \omega\ k\ H_S^2 \frac{\cosh\ (2\ k\ z)}{8\ \sinh^2 (k\ h)}$$

Where ω is the wave frequency, k the wave number, H_S is the significant wave height (the mean wave height computed from the highest third of the waves), z is the particle distance in meter above seabed and h is the mean water depth.

$$\omega = 2\pi / T$$
$$k = 2\pi / L$$

Where T and L are the wave period and wavelength, respectively and are given by:

$$L = C\ T$$
$$T = \sqrt{\frac{2\pi}{g} L \coth\left(\frac{2\pi h}{L}\right)}$$
$$C = \sqrt{\frac{g}{2\pi} L\ tgh\left(\frac{2\pi h}{L}\right)}$$

C stands for the wave celerity or the distance travelled by a crest per unit of time. These last equations are solved using a direct approximation based on Hunt's method (1979).

Two different numerical schemes have been implemented to compute the advection of the Lagrangian particles: an Euler forward method and the classical 4th order Runge-Kutta scheme. The tests carried out in the framework of the OSERIT project showed significant model results improvement of the Runge-Kutta scheme over the Euler one. For this reason, The Runge-Kutta scheme is set by default in the model.

4.3.1.2 Turbulent diffusion [only solid floater]

The turbulent diffusive transport is expressed using the random walk technique. The fluctuations velocity components (u', v' and w') are calculated following Wang et al. (2008):

$$u' = R_n \sqrt{4 K_x / \Delta t} \cos(\varphi)$$
$$v' = R_n \sqrt{4 K_y / \Delta t} \sin(\varphi)$$

Δt is the model time step; R_n is a normally distributed random number with a mean value equal to 0 and a standard deviation equal to 1; and φ is the directional angle randomly and uniformly distributed within the interval [0,π]. K_x and K_y are the turbulent diffusivity coefficients in the x and y directions, respectively.

Remark : the horizontal turbulent diffusion term is not computed when the horizontal surface spreading of surface slick is computed.

4.3.1.3 Spreading of the surface slick [liquid floaters only]

Horizontal spreading of surface slick is done in three phases. When HNS is spilled on the sea surface, it immediately spreads horizontally over the water surface due to the gravity and inertia forces and the interfacial tension between HNS and seawater. This first phase (*gravity-inertia*) lasts only a few minutes for all except the largest spill (Lehr et al. 1984). It is followed by the second phase which is known as the *gravity-viscous* spreading phase. The viscosity of the HNS opposes the gravity and inertia forces (Fingas, 2011) and the spreading process continues but slower. The third and last phase of oil spreading (known as the *surface tension-viscous* phase) starts about one week after HNS released and is therefore not considered here.

In ChemDRIFT, Fay's surface spreading is computed following Garcia et al. (1999) Monte Carlo approach:

$$u' = R_n \sqrt{\frac{4D}{\Delta t}} \cos\phi$$

$$v' = R_n \sqrt{\frac{4D}{\Delta t}} \sin\phi$$

R_n is a normally distributed random number with a mean value equal to 0 and a standard deviation equal to 1; and φ is the directional angle randomly and uniformly distributed within the interval [0,π].

During the first spreading phase, the diffusion coefficients D is computed as follows:

$$D = \frac{\pi \ k_1^2}{16} \left(\left(\frac{\rho_w - \rho_o}{\rho_w} \right) g \ V_o \right)^{1/2}$$

Where $k_1 = 1.14$ according to Fay (1971), g is the gravitational acceleration, ρ_w is the water density, ρ_o is the HNS density and V_o is the initial spill volume. This corresponds to a circular slick of radius:

$$R = \frac{k_1}{2} \left(\left(\frac{\rho_w - \rho_o}{\rho_w} \right) g \ V_o \ t^2 \right)^{1/4}$$

During the second spreading phase, the diffusion coefficients and corresponding slick radius are computed as follows:

$$D = \frac{\pi \ k_2^2}{32} \left(\frac{\left(\frac{\rho_w - \rho_o}{\rho_w} \right) g \ V_o^2}{\nu_w^{1/2}} \right)^{1/3} \frac{1}{\sqrt{t}}$$

$$R = \frac{k_2}{2} \left(\frac{\left(\frac{\rho_w - \rho_o}{\rho_w} \right) g \ V_o^2 \ t^{3/2}}{\nu_w^{1/2}} \right)^{1/6}$$

k_2 equals to 1.45 (Fay, 1971) and ν_w is the water kinematic viscosity.

4.3.1.4 Entrainment in the water column [all floaters]

Lagrangian particles can move from the sea surface into the water column through the process of vertical dispersion. Vertical dispersion is not a well understood process (Mackay and MacAuliffe, 1989) but it is agreed that it plays a major role in the oil mass exchange between the slick and the water column. It is caused by a variety of natural processes but the influence of breaking waves by which surface oil is split into droplets that are propelled into the water column, is dominant. Therefore, we decided to implement two approaches to describe the vertical exchange of the droplets from the slick to the water column.

The first approach uses an entrainment rate of surface oil into the water column that is specified by the user. This entrainment rate determines the number of particles that is randomly removed from the surface. To account for the fact that natural vertical dispersion breaks surface oil into small droplets, the radius of the dispersed oil droplets represented by the Lagrangian particles is randomnly set between 0.1 and 3 mm. The intrusion depth of the Lagrangian particle (z_H) is computed as in Guo and Wang's (2009):

$$z_H = (1.5 + 0.35 * [R]_{-1}^{1}) H_S$$

where $[R]_{-1}^{1}$ is the uniform distribution random number in the interval -1 to 1 and H_S is the significant wave height.

The second approach is very similar to the first one but uses a kinetic method based on Tkalich and Chan (2002) to compute the entrainment rate from the oil slick to the water column, λ_{ow} (1/s).

$$\lambda_{ow} = \beta \frac{k_e \ \omega \ \gamma \ H_s}{16 \ \alpha \ L_{ow}}$$

where k_e is the coefficient evaluated from experiments (usually between 0.3 and 0.5); ω is the wave frequency; γ is the dimensionless damping coefficient; H_S is the significant wave height; α is a coefficient that concerns the mixing depth of the individual particles; and L_{ow} is the vertical length-scale parameter empirically estimated to 1m. β is a coefficient that depends on HNS viscosity. $\beta = 1/\nu_o$ where the HNS viscosity is greater than 100 cSt and and $\beta = 1$ elsewhere. The parameter β mainly inhibits the natural dispersion of viscous heavy crude oil.

4.3.1.5 Beaching [all floaters]

The Lagrangian particle module includes beaching. For now, when a particle reaches a land point of the model domain, it is stopped and no re-entering is possible. Note that only surface spill is allowed.

4.3.2 Processes driving HNS spill drift and behaviour in the water column

4.3.2.1 Advection

In the water column, the advection is driven by 3D water currents $(\vec{u}_c, \omega_c)$, waves and HNS vertical slip velocity ω_0:

$$\left\langle \vec{u} \right\rangle = \alpha_c \vec{u}_c + \vec{u}_{wave} + (\omega_c + \omega_o)\vec{e}_z .$$

Slip velocity for dissolved HNS

Particles representing dissolved HNS have a neutral buoyancy and a zero slip velocity :

$$\omega_0 = 0 \text{ m/s}$$

Slip velocity for floater HNS ($\rho_0 < \rho_w$)

In the case of floaters HNS, the slip (rising) velocity is computed following Korotenko et al. (2000):

Where $\begin{cases} \omega_0 = \dfrac{g\, d^2 \left(1 - \dfrac{\rho_0}{\rho_w}\right)}{18\, \nu_w} & \text{for } d \le d_c \\ \omega_0 = \sqrt{\dfrac{8}{3} g\, d^2 \left(1 - \dfrac{\rho_0}{\rho_w}\right)} & \text{for } d > d_c \end{cases}$

And $$d_c = \frac{9.52\ \nu_w^{2/3}}{g^{1/3} (1 - \frac{\rho_0}{\rho_w})^{1/3}}.$$

ρ_0 and ρ_w are the HNS and seawater density, respectively; ν_w is the seawater viscosity; g is the gravitational constant; d is the mean diameter of the HNS liquid droplets or solid balls associated to the Lagrangian particle; and d_c is the critical diameter (~1 mm). This parameterization allows larger droplets and balls to be more buoyant and to remain longer near the surface while smaller droplets and balls are less buoyant and could be more affected by turbulence.

Slip velocity for sinker HNS ($\rho_w < \rho_o$)

In the case of floaters HNS, the slip (falling) velocity is adapted from Korotenko et al. (2000):

Where $\begin{cases} \omega_0 = \dfrac{g\, d^2 \left(1 - \dfrac{\rho_0}{\rho_w}\right)}{18\, \nu_w} & \text{for } d \le d_c \\ \omega_0 = -\sqrt{\dfrac{8}{3} g\, d^2 \left\| 1 - \dfrac{\rho_0}{\rho_w} \right\|} & \text{for } d > d_c \end{cases}$

And $$d_c = \frac{9.52\ \nu_w^{2/3}}{g^{1/3} (1 - \frac{\rho_0}{\rho_w})^{1/3}}.$$

4.3.2.2 Turbulent diffusion

The turbulent diffusive transport is expressed using the random walk technique. The fluctuations velocity components (u', v' and w') are calculated following Wang et al. (2008):

$$u' = R_n \sqrt{4 K_x / \Delta t} \cos(\varphi)$$
$$v' = R_n \sqrt{4 K_y / \Delta t} \sin(\varphi)$$
$$w' = R_n \sqrt{2 K_z / \Delta t}$$

Δt is the model time step; R_n is a normally distributed random number with a mean value equal to 0 and a standard deviation equal to 1; and φ is the directional angle randomly and uniformly distributed within the interval [0,π]. K_x and K_y are the turbulent diffusivity coefficients in the x and y directions, respectively. Their values must be specified. K_z is the vertical diffusion coefficient. It is taken from the turbulent module of the hydrodynamics model but can also be expressed as (Johansen, 1982):

$$K_z = 0.028 \left[\frac{H_S^2}{T} \right] e^{-2kz}$$

Where H_S is the significant wave height; T is the wave period; z is the vertical coordinate of oil droplets; and k is the wave number.

4.3.2.3 Resurfacing of floaters

Every floater particle ($\rho_0 < \rho_w$) that hits the sea surface is considered to have resurfaced.

For liquid floaters, all the droplets now contribute to the formation of a continuous slick at the sea surface. The droplet size diameter has no signification anymore.

For solid floaters, the size and number of grains, powder lumps or pellets do not changed.

4.3.2.4 Sedimentation of sinkers

Every sinker particle that hits the seabed is considered to have sedimented.

For liquid sinkers, all the droplets now contribute to the formation of a continuous slick covering the seabed. The droplet size diameter has no signification anymore.

For solid sinkers, the size and number of grains, powder lumps or pellets do not changed.

Once sedimented, the particle position is no more updated: no resuspension is possible.

4.3.3 Evaporation

Evaporation is computed following the Brighton model (1995) as implemented in ALOHA (ALOHA technical documentation 2013)

4.3.4 Dissolution

Dissolution is computed following the model of Mackay and Leinonen (1977), as implemented in ChemSPELL (cf. section 3.2.7).

4.4 Model output

ChemDRIFT native output file format is a netCDF file that contains for each Lagrangian particle:

- Time of release
- Position (latitude, longitude, depth)
- Drifting state (i.e. not yet released, drifting, stopped)
- State (i.e. particle on the sea surface, within the water column, beached or out of the domain)
- HNS volume of in liquid phase, in solid phase, dissolved and evaporated.

At every round hours of the simulation, ChemDRIFT also produced a netcdf file with the gridded concentration of HNS at the sea surface, in the first 3 meter of the water column, at the last 3 meters of the seabed and at the seabed.

4.5 Data processing system

With the intention to provide HNS-MS end-users with clear and straight-to-the-point information, a data processing system has been developed. This system processes the ChemDRIFT model output into a set of relevant maps and charts. From the model provided Lagrangian particles positions, it generates all kinds of maps including maps of spill trajectory, beaching risk, oil concentration, probability of presence and time residency.

ChemADEL
an atmospheric dispersion model

PAGE INTENTIONALLY LEFT BLANK

5 ChemADEL, HNS-MS atmospheric dispersion model

5.1 Introduction

In the context of a HNS release at sea, a focus is generally done on the fate of the chemical at the surface or in the water column. However some chemicals are evaporators (SEBC “E” type), so a fraction or the totally of the pollutant goes into the atmosphere. Depending on the chemical, there is a risk for human health, both for operating people on boat or helicopter, and for civilian if the release is close to the land. Hence it is important to know where the gas goes to help and prevent hazard issues.

In the project HNS-MS, the willingness is to cover all natural compartments affected by pollutant including the atmosphere. Then the purpose is to provide a simple, fast and efficient tool to evaluate the potential effects on health of a toxic gas coming from the evaporation of a HNS slick at sea surface.

The present chapter presents the mathematical models from the literature used in the ChemADEL (Chemical Atmospheric Dispersion modEL) code.

2

5.2 Mathematical model

Chemical pollutant dispersion in the atmosphere can be evaluated either with high accuracy space and time data using heavy computing methods, or with simple model providing information in an order of magnitude for decision support tool. Depending on that choice and the complexity level, three main model families exist for atmospheric dispersion of a gas cloud: Three-dimensional models (numerical), integral and Gaussian models (analytical). Both of them generally provide concentration values the atmosphere depending of elapsed time and distance from source.

In an operational context, the tool has to be quick and simple to use, so the choice has been naturally directed towards the historically and simpler Gaussian model.

The evolution of the gas cloud is governed by two physicals phenomenon: The movement and the dilution of the cloud. Parameters have strong influence on the cloud evolution, such as the type of gas (heavy, light), the meteorological conditions (wind velocity, atmospheric stability), and the environmental conditions such as ground rugosity, obstacles, relief.

The basic model equation is the scalar transport equation of the matter:

$$\frac{\partial C}{\partial t} + u\frac{\partial C}{\partial x} + v\frac{\partial C}{\partial y} + w\frac{\partial C}{\partial z} = \frac{\partial}{\partial x}\left[K_x\frac{\partial C}{\partial x}\right] + \frac{\partial}{\partial y}\left[K_y\frac{\partial C}{\partial y}\right] + \frac{\partial}{\partial z}\left[K_z\frac{\partial C}{\partial z}\right] + S + R \quad (77)$$

with C the concentration (kg.m^{-3}), (K_x, K_y, K_z) the diffusion turbulent coefficients (m^2.s^{-1}), (u, v, w) the wind velocity components (m.s^{-1}), S and R are respectively the source and sink term (kg.m^{-3}). The analytical solutions are obtained with a decomposition of the different equation terms, and with the following assumptions:

- The molecular diffusion is negligible,
- The gas is passive or neutral, which means that it has a same density as air, or is very diluted. Hence it's only submitted to the action of the air with no influence on air characteristic.
- The turbulence is homogenous and isotropic,
- The gas temperature is similar to the atmospheric temperature,
- The wind field is uniform (in velocity and direction) in time and space,
- The relative initial velocity of the leak is considered as null,
- The ground is homogenous with a low relief, with no obstacles,
- There is no deposition of pollutant, i.e. the sink term $R = 0$.

On the basis of those assumptions, three analytical formulations allow to evaluate pollutant concentration in the atmosphere, for punctual instantaneous emission of a gas, punctual long-term gas puffs emission or punctual long-term gas plume emission. Both these formulations give a distribution of concentrations in the three directions (x, y, z) following a Gaussian curve.

The domain of validity of Gaussian models is limited to a distance range of 100m – 10km, and in the case of maritime meteorological condition, in function the uniformity of the wind velocity and direction with time can't be respected beyond a couple of hour.

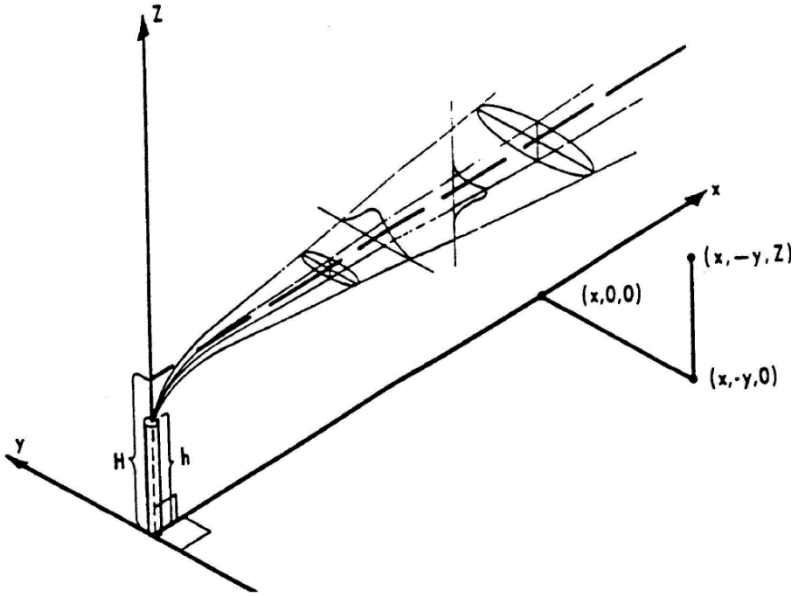

Figure 30 : Concentration Gaussian profile in a passive gas plume (Turner, 1970)

Based on what have to been done in the CLARA project, the Gaussian puff model is selected for a continuous release. The source term is provided by the evaporation flow rate of the chemical slick. In order to model the continuous release, the model considers the emission of a succession of instantaneous release (series of puffs) that will evaluate following a Gaussian distribution law in space. A wind speed or time –dependent flow is considered. The concentration is derived from the summation of all the puffs. The gas concentration C in the atmosphere at a point (x, y, z) is given as:

$$C(x,y,z,t) = \sum_{i=1}^{n} C_i(x,y,z,t_i) \tag{78}$$
$$= \sum_{i=1}^{n} \left(\frac{m_i}{(2\pi)^{2/3}\sigma_{x_i}\sigma_{y_i}\sigma_{z_i}} \right) exp\left(-\frac{[x - x_0 - u(t-t_i)]^2}{2\sigma_{x_i}^2} \right.$$
$$\left. - \frac{[y - y_0 - v(t-t_i)]^2}{2\sigma_{y_i}^2} \right) \left[exp\left(-\frac{[z - z_0 - w(t-t_i)]^2}{2\sigma_{z_i}^2} \right) \right.$$
$$\left. + \alpha\, exp\left(-\frac{[z + z_0 + w(t-t_i)]^2}{2\sigma_{z_i}^2} \right) \right]$$

with $Q(t)$ mass of the *ith* instantaneous release (kg), (u, v, w) the components of the wind velocity (ms^{-1}), n the number of considered instantaneous releases, t_i the end time of the *ith* puff emission (s), t_{i-1} the end time of the *(i-1)th* puff emission and start time of the *ith* puff (s), $(\sigma_{x_i}, \sigma_{y_i}, \sigma_{z_i})$ the standard deviation of the Gaussian distribution of the *ith* puff emission of

mass m_i relative to the localization at instant t (m), and finally α the ground reflection coefficient.

In the maritime context of HNS-MS, the ground is the sea which is not considered as a porous ground. As consequence, the reflection term is taken to the unity: $\alpha = 1$. Moreover no vertical velocity is here considered. Then we have a simplified formulation:

$$C(x,y,z) = \sum_{i=1}^{n} \left(\frac{m_i}{(2\pi)^{3/2}\sigma_{x_i}\sigma_{y_i}\sigma_{z_i}} \right) exp\left(-\frac{[x - x_0 - u(t-t_i)]^2}{2\sigma_{x_i}^2} \right) \times exp\left(-\frac{[y - y_0 - v(t-t_i)]^2}{2\sigma_{y_i}^2} \right) \times exp\left(-\frac{(z-z_0)^2 + (z+z_0)^2}{2\sigma_{z_i}^2} \right) \quad (79)$$

The time dependent mass flow rate $Q(t)$ (kg.s^{-1}) can be decomposed into n instantaneous release of mass m_i (kg), as:

$$m_i = Q\left(\frac{t_{i-1} + t_i}{2} \right)(t_i - t_{i-1}) \quad (80)$$

The *ith* instantaneous release, i indexed, is emitted at t_i and with a mass m_i. The model supposes a sufficient large number of puffs to represent the continuous plume. In ChemADEL, a puff is generated every 10 seconds, which respects numerical convergence condition.

This model is directly dependent on the standard deviation coefficients $(\sigma_{x_i}, \sigma_{y_i}, \sigma_{z_i})$. Those coefficients can be evaluated from established formula based on experimental measurements, in function of distance from source. These values correspond to time sample of 10 minutes, and to source point lower than a couple of hundred meters. The correlation of Pasquill-Turner gives the values of standard deviations depending on the Pasquill atmospheric stability classes (Table 9) and the distance from the release point:

$$\sigma = ax^b + c \quad (81)$$

with values a, b, c are reported in Table 10 and Table 11 for σ_x, σ_y and σ_z (km) respectively.

Stability classes	Mark
Extremely instable	A
Moderately instable	B
Instable	C
Neutral	D
Stable	E
Moderately stable	F
Extremely stable	G

Table 9 : Pasquill classes for atmosphere stability

Atmospheric stability (Pasquill)	a	b	c
A	0.215	0.858	0
B	0.155	0.889	
C	0.105	0.903	
D	0.068	0.908	
E	0.05	0.914	
F	0.034	0.908	

Table 10 : Coefficients relative to σ_x, σ_y

Atmospheric stability (Pasquill)	a	b	c
A	0.467	1.89	0.01
B	0.103	1.11	0
C	0.066	0.915	0
D	0.0315	0.822	0
E (x < 1km)	0.0232	0.745	0
E (x > 1km)	0.148	0.15	-0.126
F (x < 1km)	0.0144	0.727	0
F (x > 1km)	0.0312	0.306	-0.017

Table 11 : Coefficients relative to σ_z

Pasquill's classes described the atmospheric stability, and can be evaluated from wind velocity, solar insolation and cloud nebulosity. The methods to calculate the stability class have been implemented in ChemADEL (ALOHA 5.4.4 technical description): It consists in determining the solar insolation from cloudiness index and the location/time of the release. Then depending on insolation (day/night context) and on wind speed, the stability mark is given by an established table.

Wind speed	Day			Night	
At 10 meters (m/s)	Solar insolation			Cloud cover	
	Strong	Moderate	Slight	>50%	<50%
<2	A	A-B	B	E	F
2-3	A-B	B	C	E	F
3-5	B	B-C	C	D	E
5-6	C	C-D	D	D	D
>6	C	D	D	D	D

Table 12 : Solar insolation and stability class table (ALOHA 5.4.4 Technical documentation)

The strong/moderate/slight solar insolation are described by a computed insolation greater than 851 W/m², between 851 and 526 W/m², and between 526 and 176 W/m² respectively. The solar insolation is estimated by:

$$F_s = \begin{cases} 1111(1 - 0.0071C_I^2)(\sin\phi_s - 0.1) & \sin\phi_s > 0.1 \\ 0 & otherwise \end{cases} \quad (82)$$

with C_I the cloudiness index (on a scale of 0 to 10) and ϕ_s the solar altitude (angle of the sun above the local horizon) in degrees. This one is evaluated by:

$$\sin\phi_s = \sin\theta \sin\delta_s + \cos\theta \cos\delta_s \cos h_s \tag{83}$$

with

$$\delta_s = 23.45\left(\frac{2\pi}{360}\right)\sin\left(\left(\frac{2\pi}{360}\right)0.986(J-80)\right) \tag{84}$$

and

$$h_s = \left(\frac{2\pi}{360}\right)\left[15\left(12-\left(Z-\frac{\lambda}{15}\right)\right)\right] \tag{85}$$

the latitude θ (rad), the longitude λ (rad), Z the hour of the day in Greenwich Mean Time (GMT), and J the Julian day (day number in the year, in days).

References

PAGE INTENTIONALLY LEFT BLANK

References

ALOHA (Areal Locations Of Hazardous Atmospheres) 5.4.4, technical description, NOAA Technical Memorandum NOS OR&R 43.

Aprin, L., Slangen, P., 2015, Chemical Modelling Description in CLARA Project, HNS-MS technical report.

Aprin, L., 2016, Characterization of the HNS behaviour in the water column, HNS-MS technical report.

Aprin, L., 2016, Modelisation of draining mechanism for submerged vessel filled with chemical, HNS-MS technical report.

Aprin, L., Slangen, P., 2015, Chemical Modelling Description in CLARA Project.

Arcopol plus, Fernandes R., 2012, Technical Report on HNS model implementation.

Bonn Agreement (2016) Bonn Agreement Counter-Pollution Manual. Chapter 20: Inventory of Assessment Tools.

Chemmap version 6.10, 2014, Technical User's Manual 2014.

Clift R., Grace J.R., Weber M.E., 1978, Bubbles, drops and particles, Academic Press, New York.

Daniel P., F. Marty, P. Josse, C. Skandrani and R. Benshila (2003) Improvement of drift calculation in MOTHY operational oil spill prediction system, Proceedings of the 2003 International Oil Spill Conference, American Petroleum Institute, Washington, D.C.

Dasanayaka L., Yapa P.D., 2009, Role of plume dynamics phase in a deepwater oil and gasl release model, Journal of Hydro-environment Research 2, 243-253.

Dodge, F., Park, J., Buckingham, J., and Magott, R., 1985, Revision and experimental verification of the hazard assessment computer system models for spreading, movement, dissolution, and dissipation of insoluble chemicals spilled onto water. Report: CG-D-35-83. Washington.

Dodge, F. T., Bowlles, E. B., White, R. E., & Flessner, M. F. (1980). Release rates of hazardous chemicals from a damaged cargo vessel. In Proceedings of the 1980 National Conference on Control of Hazardous Material Spills, May 13–15, 1980 (pp. 381–385). Nashville, TN: Vanderbilt University.

Dulière, V., F. Ovidio and S. Legrand (2013) Development of an integrated software for forecasting the impacts of accidental oil pollution - OSERIT. Final Report. Brussels: Belgian Sciences Policy Office, 65 p.

Fernandez M.I., 2013, Modelling spreading, vaporisation and dissolution of multi-component pools, PhD thesis submitted to University College London.

Garcia-Matinez, R. and H. Flores-Tovar (1999) Computer Modeling of Oil Spill Trajectories with a high Accuracy Method. Spill Science & Technology Bulletin, 5 (5/6), pp. 323-330.

Guo, W.J. and Y.X. Wang (2009) A numerical oil spill model based on a hybrid method. Marine Pollution Bulletin, 58, pp. 726-734.

Hayduk, W., and Laudie H., 1974, Prediction of diffusion-coefficients for nonelectrolytes in dilute aqueous-solutions, AIChE J., 20, 611 – 615.

INERIS, Direction des Risques Accidentels, 2002, Méthodes pour l'évaluation et la prévention des risques accidentels (DRA-006), Ministère de l'écologie et du développement durable.

Johnson, A. I., Besik, F., and Hamielec, A. E., 1969, "Mass transfer from a single rising bubble." Can. J. Chem. Engrg., 47, 559–564.

King, M.B., 1969, Phase Equilibrium in Mixtures. Pergamon, Oxford.

Kumar, A., Hartland, S., 1999, Correlations for prediction of mass transfer coefficients in single drop systems and liquid–liquid extraction columns, Chem. Eng. Res. Des. 77, 372–384.

Lee J. H. W.; Cheung V. 1990, Generalized Lagrangian model for buoyant jets in current, Journal of Environmental Engineering, vol.116.

MacKay, D. and Leinonen, P.J., 1977, Mathematical model of the behaviour of oil spills on water with natural and chemical dispersion. Report EPS-3-EC-77-19.

McGinnis, D. F., Greinert, J. , Artemov, Y. , Beaubien, S. E. , and Wuëst, A., 2006, Fate of rising methane bubbles in stratified waters: How much methane reaches the atmosphere? Journal of Geophysical Research, Vol. 111.

Poling, B.E, Prausnitz, J.M, O'Connell, J.P., 2001, The properties of gases and liquids, fifth edition, McGraw-Hill.

Tkalich, P., and E.S. Chan, 2002. Vertical mixing of oil droplets by breaking waves. Marine Pollution Bulletin, 44, pp. 1219-1229.

Wang, S.D., Y.M. Shen, Y.K. Guo, and J. Tang, 2008: Three-dimensional numerical simulation for transport of oil spills in seas. Ocean Engineering, 35, pp. 503-510.

Wegener, M., Paul, N., Kraume, M., 2014, Fluid dynamics and mass transfer at single droplets in liquid/liquid Systems, International Journal of Heat and Mass Transfer 71, 475-495.

Weiss, R.F., 1974, Carbon dioxide in water and seawater: The solubility of a non-ideal gas. Marine Chemistry, 2, 203-215.

Witlox, H., 2008, *PVAP- Theory document.* London: DNV Technica (Phast Technical Reference).

Wüest, A., Brooks, N.H., Imboden, D.M., 1992, Bubble plume modeling for lake restoration. Water resources Research 28 (12), 3235-3250.

Yamamoto, S., Alcauskas, J.B., Crozier, T.E., 1976, Solubility of methane in distilled water and seawater. Journal of Chemical and Engineering Data 21 (1), 78– 80.

Yapa, P.D., 1994, Oil Spill Processes and Model Development, Journal of Advanced Marine Technology, AMTEC, Tokyo, Japan, March, 1-22.

Yapa, D.P. and Zheng L., 1997, Simulation of oil spills from underwater accidents I: Model development, Journal of Hydraulic Research, vol. 35.

Zheng, L., Yapa, P.D., 2000a, Buoyant velocity of spherical and non-spherical bubbles/droplets. Journal of Hydraulic Engineering, ASCE 126 (11), 852– 854.

Zheng, L., Yapa, P.D., 2002, Modeling gas dissolution in deepwater oil/gas spills. Journal of Marine Systems 31, 299– 309.

PAGE INTENTIONALLY LEFT BLANK

Annexes

PAGE INTENTIONALLY LEFT BLANK

Annex 1 Implementation notes on ChemSPELL the near field model

ChemSPELL (Chemical Subsea Plume modEL for Leakage) is a comprehensive model developed by Alyotech to perform simulations and provide a source term to the HNS far-field model in release scenario such as wells or pipeline blowout, but also for sunken vessels. The technical description is given in Figure 31.

Programming languages	C++, Qt Framework
Executables binaries	64 bits
Operating systems	Debian 8 "Jessie" 64 bits CentOS 6.5 64 bits Windows 7 64 bits

Figure 31 : ChemSPELL technical description

In order to run ChemSpell, the path to ChemSPELL libraries has to be added to the library path. Line call example is given in Figure 32.

```
export LD_LIBRARY_PATH=/my/path/to/libraries
./chemspell /my/path/to/configurationFile.txt /my/path/to/copernicusOceanicData.nc
```

Figure 32 : ChemSPELL call example

As input parameters, two files are read:

- The simulation parameters (simulation start/stop time, release position, volume, HNS properties, etc.). Details are given in Table 13.
- The *COPERNICUS* extracted file containing the oceanic data needed by the tool (temperature, salinity and current profiles along the water column). Details are given in Table 14.

Simulation is run until the simulation time exceeds the simulation stop time (Figure 33). Finally an output NetCDF4 file is created. It contains relevant data of the HNS in the water column (Table 15). The grid is based on particles extremum positions, with a determined mesh size of 10'' DD (lat/lon) by 1m depth.

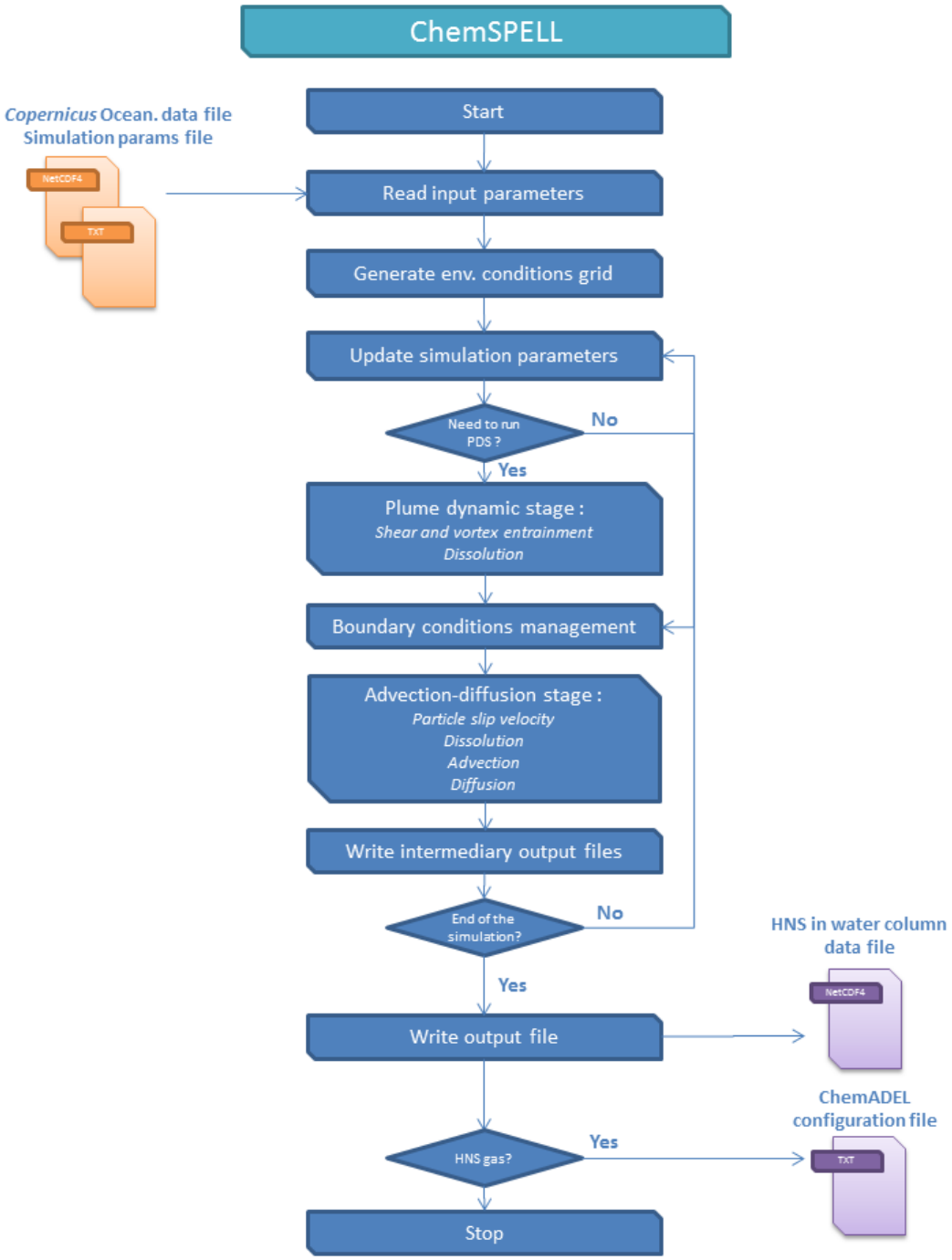

Figure 33 : ChemSPELL (near-field model) flow diagram

Parameters	Units	Format/Value
HNS name	-	string
HNS chemical formula	-	string
HNS SEBC	-	Combination of "D", "E", "G", "S", "F"
HNS phase	-	L or G
HNS molar mass	$kg.mol^{-1}$	numeric
HNS solubility	$mol.m^{-3}$	numeric
Water-HNS interfacial tension	Pa.s	numeric
HNS kinematic viscosity	$m^2.s^{-1}$	numeric
HNS density	$kg.m^{-3}$	numeric
HNS critical temperature (if gas)	K	numeric
HNS critical pressure (if gas)	Pa	numeric
HNS acentric factor (if gas)	-	numeric
Simulation/release start time	UTC	*AAAA-MM-JJTHH:mm:ssZ*
Simulation stop time	UTC	*AAAA-MM-JJTHH:mm:ssZ*
Simulation label	-	string
Release latitude	DD	numeric
Release longitude	DD	numeric
Release depth	m	numeric
Breach diameter	m	numeric
Break height	m	numeric
Tank volume	m3	numeric
Tank height	m	numeric
Tank single breach	-	1 simple 0 double
HNS temperature at breach	K	numeric
Flow rate (normalised if gas)	$(N)m^3.s^{-1}$	numeric
Breach angle with Ox axis	rad	numeric
Breach angle with Oxy plan	rad	numeric
Scenario type	-	0 sunkenVessels, 1 wells, 2 pipelines
Dissolution process	-	0 off, 1 on
Ouput directory	-	string
Mesh size	m	numeric
Number of parcels		numeric
ChemADEL configuration file (if gas)	-	string

Table 13 : Parameters from ChemSPELL simulation configuration file

Parameters	Units	Dimensions
Salinity	PSU	time, depth, lat, lon
Temperature	K	time, depth, lat, lon
South-North current	$m.s^{-1}$	time, depth, lat, lon
West-East current	$m.s^{-1}$	time, depth, lat, lon
Sea surface height above geoid	m	time, depth, lat, lon

Table 14 : Parameters from oceanic COPERNICUS netCDF4 data file

Parameters	Units	Dimensions
HNS concentration	$kg.m^{-3}$	time, depth, lat, lon
HNS mass	kg	time, depth, lat, lon
HNS volume	m^3	time, depth, lat, lon
HNS flow rate	$m^3.s^{-1}$	time, depth, lat, lon
Number of HNS particle	-	time, depth, lat, lon
Dissolved HNS concentration	$kg.m^{-3}$	time, depth, lat, lon
Dissolved HNS mass	kg	time, depth, lat, lon
Dissolved HNS volume	m^3	time, depth, lat, lon
Dissolved HNS flow rate	$m^3.s^{-1}$	time, depth, lat, lon
Number of dissolved HNS particle	-	time, depth, lat, lon
Particle size distribution	-	class, time, depth, lat, lon

Table 15 : Parameters from ChemSPELL netCDF4 data file

Annex 2 Implementation notes on ChemADEL atmospheric dispersion model

ChemADEL (Chemical Atmospherical Dispersion modEL) is a mathematical model developed by Alyotech to perform simulations of the HNS dispersion in the atmosphere, when the release chemical at surface is of type evaporating. The technical description is given in Figure 34

Programming languages	C++, Qt Framework
Executables binaries	64 bits
Operating systems	Debian 8 "Jessie" 64 bits CentOS 6.5 64 bits Windows 7 64 bits

Figure 34 : ChemADEL technical description

In order to run ChemADEL, the path to ChemADEL libraries has to be added to the library path. Line call example is given in Figure 35Figure 32.

```
export LD_LIBRARY_PAT=/my/path/to/libraries
./chemADEL /my/path/to/configurationFile.txt /my/path/to/meteorologicData.nc
```

Figure 35 : ChemADEL call example

As input parameters, two files are read:

- The simulation parameters (simulation start/stop time, release position, evaporation rate, grid size and mesh cell). Details are given in Table 13.
- The *meteorological extracted* file containing the atmospheric data needed by the tool (wind velocity components, etc.). Details are given in Table 14.

Simulation is run until the simulation time exceeds the simulation stop time (Figure 36). Finally an output NetCDF4 file is created. It contains relevant data of the HNS in the atmosphere (Table 15).

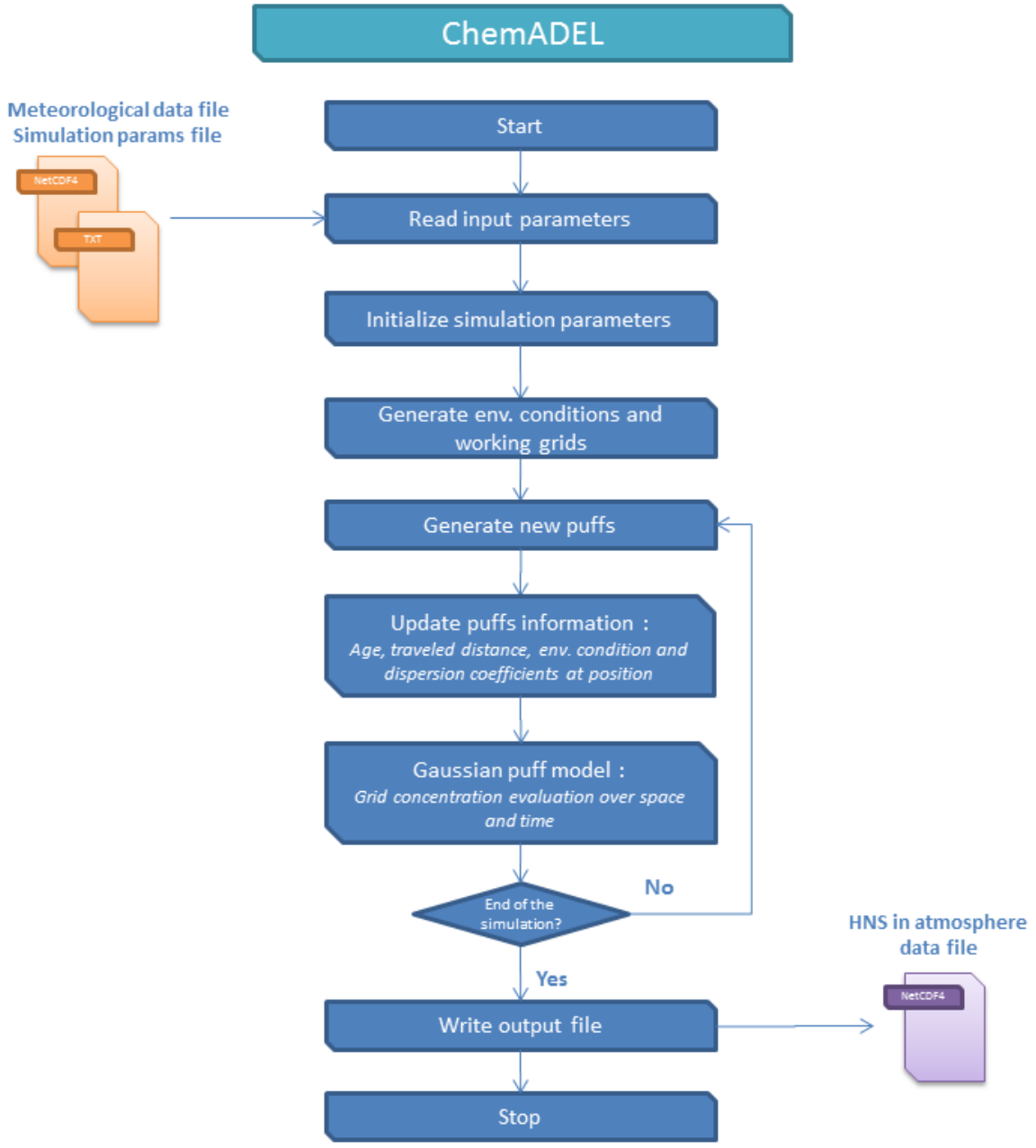

Figure 36 : ChemADEL flow diagram

Parameters	Units	Format/Value
Simulation/release start time	UTC	*AAAA-MM-JJTHH:mm:ssZ*
Simulation stop time	UTC	*AAAA-MM-JJTHH:mm:ssZ*
Simulation label	-	string
Release latitude	DD	numeric
Release longitude	DD	numeric
Mass flow rate	$kg.s^{-1}$	numeric
Ouput directory	-	string
Mesh size	m	numeric
Grid size	m	numeric

Table 16 : Parameters from ChemADEL simulation configuration file

Parameters	Units	Dimensions
Wind component *u* at 10m	$m.s^{-1}$	time, lat, lon
Wind component *v* at 10m	$m.s^{-1}$	time, lat, lon
Temperature at 2m	K	time, lat, lon
Accumulation	m	time, lat, lon
High cloud coverage index	-	time, lat, lon
Medium cloud coverage index	-	time, lat, lon
low cloud coverage index	-	time, lat, lon
Pressure	Pa	-
Mean sea level pressure	Pa	time, lat, lon
Specific humidity	$kg.kg^{-1}$	time, lat, lon

Table 17 : Parameters from meteorological netCDF4 data file

Parameters	Units	Dimensions
HNS concentration	$kg.m^{-3}$	time, depth, lat, lon

Table 18 : Parameters from ChemADEL netCDF4 data file

Improving Member States preparedness
to face an HNS pollution of the Marine System